Environmental Science Nano

ROYAL SOCIETY OF CHEMISTRY

PAPER

View Article Online
View Journal | View Issue

Check for updates

Cite this: *Environ. Sci.: Nano*, 2024, 11, 2521

Functional silver-based nanomaterials affecting zebrafish development: the adverse outcomes in relation to the nanoparticle physical and chemical structure†

Patrizia Bonfanti, ‡*[a] Anita Colombo,‡[a] Rossella Bengalli, [a] Maurizio Gualtieri,[a] Ilaria Zanoni, [b] Magda Blosi,[b] Anna Costa[b] and Paride Mantecca*[a]

Received 10th November 2023,
Accepted 10th April 2024

DOI: 10.1039/d3en00813d

rsc.li/es-nano

The growing demand for effective antimicrobials determined a significant increase of new nanoformulated materials to fight against bacteria and viruses, to be used in many industrial sectors including textiles, cosmetics, pharmaceuticals, and air and water filtering. Nano silver (Ag)-based materials, well-known for their antibacterial properties, are among the most exploited ones. However, the toxicity mechanisms of Ag nanoparticles (NPs) are still debated, requiring more evidence to support a safe-by-design (SbD) strategy for these materials. This study used zebrafish (*D. rerio*) to assess and compare the toxic and adverse effects (AEs) of commercial Ag-NPs (naked and PVP-coated) and newly synthesized hydroxyethylcellulose-coated Ag-NPs in solution (Ag-HECs) or the powder (Ag-HECp) form. Statistical correlation analysis between AEs and NP physico-chemical (p-chem) properties, such as size, surface charge, and solubility, was also performed. The results ranked the materials as follows in terms of acute lethality (LC_{50}) and malformation (EC_{50}) effects: Ag-HECp > Ag-HECs > Ag-PVP > Ag-NKD. Notable AEs included axial defects, pericardial edema, and reduced lipid yolk consumption, impacting embryo growth and hatching time. Correlation analyses showed that the stabilizing agent HEC, though a safe polymer, played a significant role in modulating Ag-NPs' reactivity toward embryonic structures. The study discusses the biological mode of action and potential molecular events underlying the observed effects. These findings contribute to understanding the biological targets and AEs modulated by tuning Ag-NPs' properties and will additionally feed the SbD frameworks under development for implementing safe and sustainable Ag-based nano-enabled antimicrobial materials.

Environmental significance

Antimicrobial silver-based NPs embedded in the eco-friendly biopolymer hydroxyethyl cellulose (Ag-HECs) were conceived in a safety-by-design framework, aiming to efficiently combat bacteria and viruses while minimizing impact on non-target organisms. Zebrafish embryos, used to bridge *in vitro* and *in vivo* studies, highlighted that the novel Ag-NPs did not show improved safety compared to commercial Ag-NPs, when considering acute toxicity and relevant adverse effects (AEs). Correlation analysis between AEs and NPs' p-chem properties revealed that the NP surface chemistry and positive ζ potential were crucial factors affecting the reactivity towards zebrafish and pointed out the possibility of making Ag-NPs safer by tuning such properties. This finding provides valuable insights for optimizing nanomaterial design to minimize harm to human and environmental health.

1. Introduction

The nanotechnological market is rapidly expanding all over the world, allowing great advantages in the production of many consumer goods with improved efficacy in many industrial sectors. One of the main fields where nanomaterials (NMs) find fertile ground for their application is the production of new antimicrobials. This in fact represents a high demanding sector for novel materials and coatings capable of fighting the spread of bacterial infection, including those caused by the steadily growing antibiotic-resistant strains as well as addressing the emergence of viral

[a] *Research Centre POLARIS (Environmental Health & Sustainability), Dipartimento di Scienze dell'Ambiente e della Terra, University of Milano Bicocca, Piazza della Scienza 1, 20126 Milano, Italy. E-mail: patrizia.bonfanti@unimib.it, paride.mantecca@unimib.it*

[b] *National Research Council of Italy (CNR-ISSMC, former ISTEC), Istituto di Scienza, Tecnologia e Sostenibilità per lo Sviluppo dei Materiali Ceramici, Via Granarolo 64, 48018 Faenza, Italy*

† Electronic supplementary information (ESI) available. See DOI: https://doi.org/10.1039/d3en00813d

‡ These authors contributed equally to this work.

infections such as SARS-CoV-2.[1,2] In this respect, many NMs are under scrutiny for their ability to kill bacteria and inactivate viruses basing on their biological reactivity. In particular, metal and metal oxide nanoparticles (NPs), like Ag, CuO, ZnO, MgO, and TiO_2, can provide long-term antibacterial and antibiofilm effects through the production of reactive oxygen species (ROS) that are able to induce damage to cellular structures, metabolic pathways, and DNA replication in bacterial cells.[3] Moreover, it has been evidenced that, thanks to their efficient ROS-mediated cytotoxicity, resulting in bacterial growth inhibition, metallic NPs induced an attenuation in antibiotic resistance gene transfer.[4] These findings push toward an increasing use of metallic NMs for developing new antimicrobials. Nonetheless, concerns about their human and eco-toxicity are slowing down their application and access to the market. Thus, for NMs to be used in daily healthcare and other industrial applications, such as antimicrobial textiles and depolluting and antibiofilm air and water filters, a key challenge is to ensure human and environmental safety, preventing or minimizing NM toxicity. A suitable approach to guarantee such characteristics to new nano-antimicrobials is represented by the safe-by-design (SbD) strategy, which is based on the possibility to design and re-design materials and processes during the initial stages of product development, to minimize exposure and hazards, while optimizing the efficacy.[5,6] In the framework of the EU H2020 project ASINA, Ag-based NMs are developed and investigated for producing functional antimicrobial textiles and cosmetics, according to SbD principles. To implement the strategy, both NMs and nano-enabled products (NEPs) containing Ag-NPs are being optimized to achieve efficient, but safe antimicrobial activities. In a recent review on the effects and mode of action of Ag-NPs in bacteria, human cells and *in vivo* systems, it is underlined how the exact bactericidal and cytotoxic mechanisms of Ag-NPs remain almost unclear.[7] They may arise from either Ag-NPs themselves or released Ag ions; the final cytotoxic effects have been reported to be dose-, size- and time-dependent.[8,9] Nevertheless, Ag-NP toxicity to both prokaryotic and eukaryotic cells strictly depends on the particle physico-chemical (p-chem) properties and in particular on the surface reactivity.[10] These authors reported that the structural properties of the NPs might influence the release of Ag^+ ions, which ultimately are the key players of the NP surface oxidative potential and the consequent cellular toxicity. This gives reason to the many efforts still in place to find out the best modality to synthesize and tune the surface properties for engineering Ag-NPs, with the final aim of improving their antibacterial action without increasing their toxic effects on human cells and on environmental organisms.

Noteworthily, the surface modification may significantly modulate the Ag-NP toxic effects even more than other parameters. Studying the effects of Ag-NPs coated with polyvinylpyrrolidone (PVP), citrate, citrate-tannic acid, citrate-gluthathione or gum arabic on Japanese medaka (*Oryzias latipes*), Kwok *et al.* demonstrated that the Ag dissolution largely depended on the NP size, but the toxicity was mainly affected by the NP aggregation behaviour, which in turn was a result of the properties dictated by the coating materials.[11] Similarly, citrate- and branched polyethylenimine (BPEI)-coated Ag-NPs displayed different embryotoxic and teratogenic effects on exposed *Xenopus laevis* embryos, as a consequence of the enhanced capability of the positively charged BPEI-Ag-NPs to interact with and affect embryonic tissues.[12] In *in vitro* cultured murine RAW 264.7 macrophages, 20 nm and 50 nm Ag-NPs coated with bovine serum albumin (BSA), PVP and chitosan influenced TNF-α and ROS production, with the negatively charged BSA-Ag-NPs being the more potent in inducing the adverse effects.[13] In HepG2 cells treated with Ag-NPs modified with sodium bis(2-ethylhexyl)-sulfosuccinate, cetyltrimethylammonium bromide, PVP, poly-L-lysine and BSA, both uptake and cytotoxicity were significantly affected by the coating, again with the BSA-Ag-NPs being the most toxic, although no clear correlations with the particle surface charge were identified.[14] Taken together, these results evidence how Ag-based hybrid NMs, usually obtained by surface modification with polymers, are worthy of additional efforts in view of characterizing the hazard profile and the role of the modifying agent in orienting the mechanisms of toxicity.

The possibility to generate new hybrid NMs takes advantage of an almost infinite variety of combinations between *e.g.* metal NPs and synthetic or bio-based polymers, which make the option of case-by-case biological testing on traditional mammalian models unfeasible, since they are cost- and time-consuming. In this sense, the use of zebrafish (*Danio rerio*) embryos may provide significant contributions for alternative nanotoxicity screening using a whole organism model that can bridge the gap between *in vitro* and mammalian biocompatibility studies. This vertebrate developmental *in vivo* model is relevant in aquatic toxicity studies, as well as in predictive mechanistic human toxicology,[15] while Noyes *et al.* suggested zebrafish as a powerful and easy-to-use *in vivo* model for sustainable chemical design.[16] It has been also definitely established as a valuable model for NP toxicity assessment,[17] with several published papers also reporting on the adverse effects of Ag-NPs.[18–21] The size, with smaller particles being the most toxic, and dissolution of Ag ions seem to be the most important factors driving the Ag-NP toxicity in zebrafish.[22,23] By adopting a toxicogenomic approach, the last authors reported that the main molecular events affected are oxidative phosphorylation and protein synthesis, independent from the nano-, bulk and ionic form of Ag, thus suggesting a common mechanism of action. Despite the huge efforts put in the last ten years to elucidate the Ag-NP toxicity, relatively few papers specifically address the interplay between the metallic core and the polymer surface coating in determining the hazard profile and the toxicity mechanisms of hybrid NMs in zebrafish. Nonetheless, this represents a crucial aspect for the synthesis and

application of new Ag-based nano-antimicrobials, following the SbD framework.

To this end, in this study, the hazard profile of newly synthesized hydroxyethylcellulose (HEC)-coated Ag-NPs, obtained in solution (Ag-HECs) or the powder (Ag-HECp) form, was evaluated and compared to that of commercially available polyvinylpyrrolidone (PVP)-coated Ag-NPs (Ag-PVP) and naked Ag-NPs (Ag-NKD) on zebrafish embryos. The synthesized Ag-HEC NPs have previously demonstrated their antimicrobial activity (against both Gram + and − bacteria, *E. coli* and *S. aureus* respectively, and viruses, Sars-Cov-2),[24] making them promising candidates for fighting resistant pathogens. Moreover, the Ag-HEC NPs are derived from a single-step, environmentally friendly synthesis, performed at room temperature, and their efficacy is guaranteed even at low concentrations, making them promising NMs also from a perspective of sustainability.[24] HEC, known for its intrinsic antibacterial properties, serves as a benign agent and is particularly effective in stabilizing Ag-NPs in water, allowing their use in manufacturing processes (*e.g.* spray coating) for their incorporation in nano-enabled products (NEPs), such as textile or cosmetic products with antibacterial and antiviral properties, and their application also in hospitals.[25,26]

After the p-chem characterization of the NPs and the suspensions, the fish embryo acute toxicity (FET) test[27] was performed to determine the concentration-dependent toxic responses, as well as the comparative lethal and teratogenic concentrations. To promote the knowledge and implementation of the SbD approach, the main adverse morphological outcomes have been characterized and correlated with the particles' p-chem properties.

2. Materials and methods

2.1. Ag nanoparticles

Naked silver-nanopowder (Ag-NKD) (99% trace metal basis, CAS number 484059) and silver-nanopowder containing polyvinylpyrrolidone as a coating agent (Ag-PVP) (99.5% trace metal, CAS number 576832) were purchased from Sigma-Aldrich and used as reference materials for a comparative toxicological analysis with the ASINA produced NMs. As reported in the product datasheet, the primary size of Ag-NKD and Ag-PVP NPs was <150 nm and <100 nm, respectively. ASINA NPs, kindly provided by the Italian National Research Council (ISSMC-CNR, former ISTEC-CNR, Faenza, Italy), are Ag coated with hydroxyethyl cellulose (HEC), obtained in suspension or in the powder form (referred to in the text as Ag-HECs and Ag-HECp, respectively), as previously described.[24,26,28,29] The Ag concentration in suspension was equal to 0.5% wt in Ag-HECs and 7.18% wt in Ag-HECp. The detailed characterization of these novel NPs reported by Motta *et al.* revealed a rather narrow primary size distribution for both Ag-HECs and Ag-HECp NPs (3–20 nm and 5–50 nm for Ag-HECs and Ag-HECp, respectively).[30]

2.2. Preparation and characterization of Ag-NP suspensions

Stock suspensions were prepared according to a standardized dispersion protocol established in the ASINA project.[30] Briefly, stocks of 1 mg Ag mL^{-1} Ag-NPs were prepared in sterile MilliQ water as follows. Ag-NKD and Ag-PVP were weighed, and the suspensions were dispersed by sonication cycles (1 s pulse, 1 s pause) for 10 min using a probe-type ultrasonic homogeniser (Sonopuls HD3100, Bandelin, Berlin, Germany), operating at 40 W. Ag-HEC stock suspension was vortexed for 30 s and directly diluted in MilliQ water to reach the desired concentration. Ag-HECp powder was weighed, left to set overnight in the appropriate volume of MilliQ water and then vortexed for 30–60 s. No sonication was applied for the two Ag-HEC NPs. Ag-NP stock solutions were kept at +4 °C in the dark and used for analysis within one month.

Dynamic light scattering (DLS), transmission electron microscopy (TEM) and inductively coupled plasma optical emission spectrometry (ICP-OES) analyses were used to characterize Ag-NP suspensions in terms of size, shape, surface charge (ζ-potential), agglomeration state and dissolution.

TEM analyses were performed on Ag-NP suspensions prepared in MilliQ water at a concentration of 100 μg mL^{-1}; five μL of suspension was deposited on a TEM grid (Formvar-carbon support film, 200 mesh, copper) and left to dry overnight. All the samples were observed under a Jeol Jem 2100 Plus TEM microscope (Jeol Ltd., Tokio, Japan).

For DLS analysis, Ag-NP stock suspensions were vortexed and diluted in distilled water (DI) and embryo rearing solution (FET solution) (in mg L^{-1}: $NaHCO_3$ 100, Instant Ocean salt 100, $CaSO_4$ 190) to obtain the concentration of 10 and 100 mg L^{-1} for Ag-NKD and Ag-PVP and 10 mg L^{-1} for Ag-HECs and Ag-HECp. All the suspensions were analysed using a Zetasizer Nano ZS90 (Malvern Ltd., Warwickshire, UK) at time 0, just after preparation, and after 24 h and 96 h of incubation at 25 °C to assess the NP stability in suspension for the entire duration of the FET test. Three independent suspensions for each NP were run in triplicate to obtain the average hydrodynamic diameter (D_h), size distribution based on the polydispersity index (PdI) and ζ-potential measurements.

ICP-OES analysis was performed to assess the release of Ag^+ from NPs in FET solution. Briefly, Ag-NP suspensions prepared in FET solution at concentrations of 1–10 and 100 mg L^{-1} were sampled under static conditions (without further shaking of the starting suspensions) at three time points (t0, t24 and t96 h), representing the conditions of exposure of the embryos. Samples were filtered through 10 kDa molecular weight cut-off membranes (4500 rpm for 45 min) and the filtered solutions were analysed by ICP-OES coupled with a OneNeb nebulizer (ICP-OES 5100 vertical dual view apparatus-Agilent Technologies, Santa Clara, CA, USA). The analysis was performed in radial viewing mode, and calibration curves were obtained with 0.1, 1.0, 10.0 and 100.0 mg L^{-1} standards for the Ag element (PerkinElmer 1 mg L^{-1}

Ag in 2% HNO_3, N9304265). Nitric acid was added to standards and diluted samples (1 : 10 v/v).

2.3. Fish embryo toxicity test

Wild-type zebrafish (AB strain) were maintained as described in the ESI† (Materials and methods S2). All experiments were performed on embryos within 120 h post fertilization (hpf), thus were not subject to animal experimentation rules according to European and Italian directives.[31] To obtain critical concentrations able to incite nanotoxicity in 50% of 96 hpf zebrafish embryos, a fish embryo toxicity (FET) test was set up following the OECD guideline n. 236 (ref. 27) with minor modification.

Briefly, groups of 20 zebrafish embryos at the same developmental stage (3 hpf) were selected and randomly transferred into Petri dishes (Ø 6.0 cm) (5 embryos per dish) containing 10 mL of FET solution (control group) or Ag-NP suspensions at different concentrations. Based on previous range finding tests, nine fresh final working concentrations considering the Ag mass range of 0.1–100 mg L^{-1} for Ag-NKD and Ag-PVP and 0.1–15 mg L^{-1} for Ag-HECs and Ag-HECp were prepared in FET solution starting from sonicated (Ag-NKD and Ag-PVP) or vortexed (Ag-HECs and Ag-HECp) stock solutions. The suspensions were vortexed for 30 s prior to use to obtain homogeneous dispersion of particles. The solution with the stabilizer HEC at two concentrations (1 and 10 mg L^{-1}), equivalent to those of Ag-HEC NP suspensions, was also tested by FET to identify its potential toxicity. Embryos were exposed in a thermostatic chamber (Piardi, Italy) at 26 ± 0.5 °C, under static conditions.

Lethal endpoints (coagulation, lack of somite formation, lack of tail detachment from the yolk sac, lack of the heartbeat) indicating acute toxicity were monitored daily until the end of the test (96 hpf). Hatching rates of all treatment and control groups were recorded in embryos at 48, 72 and 96 hpf.

Moreover, to assess whether exposure to Ag-NPs affected the organogenesis, a list of phenotypes representative of morphological endpoints to evaluate teratogenicity was considered (see Table 3).

At least three independent exposure experiments were performed and the experiments were considered valid only if the survival rate in the control embryos was ≥90%. At the end of experiments, the mortality index, the percentage of altered phenotypes among survivors and the hatching rate were determined to obtain the median lethal concentration (LC_{50}), the median effective concentration (EC_{50}) and the median hatching time (HT_{50}), respectively.

2.4. Ag uptake quantification in embryos

Accumulation of Ag was performed in 96 hpf zebrafish larvae exposed to 10 mg L^{-1} (Ag-NKD and Ag-PVP) and 1 mg L^{-1} (Ag-HECs and Ag-HECp) concentrations corresponding to at least one third of the calculated LC_{50}. Larvae (pools of 50 animals; n = 3 experimental replicates per treatment) were collected at the end of the FET test and processed according to Boyle and Goss.[32] Briefly, after being transferred to 15 mL tubes and washed 4 times with an excess of NaCl (2.9 g L^{-1}) to remove Ag bound to the body surface, zebrafish were rinsed in MilliQ water and stored in dry ice until requested. For Ag quantification, larvae were treated by adding 0.25 mL of nitric acid and 0.25 mL of hydrogen peroxide to each sample. The digested mixture was added to 2.5 mL of MilliQ water and then analyzed by ICP-OES coupled with a OneNeb nebulizer (ICP-OES 5100—vertical dual view apparatus – Agilent Technologies, Santa Clara, CA, USA). The analysis was performed as described in section 2.2.

2.5. Morphometric analyses

At the end of each FET test, a subset of ten 96 hpf zebrafish larvae were randomly collected from each experimental group (in total at least n = 30), anesthetized in 0.016% tricaine methanesulfonate (MS-222) and fixed in 10% neutral buffered formalin. Photomicrographs in lateral (left side) and dorsal view of the larvae mounted in 3% methylcellulose were taken using a stereomicroscope Zeiss (Stemi SV6) equipped with a digital camera (Axio Cam ERc5s). Digital images were processed with Zen 3.4 (blue edition) software to quantify the following morphometric features: body length (distance from the tip of Meckel's cartilage to the tail tip), eye size (area and longitudinal diameter), yolk sac area and head width (see Fig. 6A). Morphological parameters were not measured at the highest exposure concentrations when the mortality rates were higher than 90%.

2.6. Morphological and elemental analyses of the chorion by scanning electron microscopy (SEM)

For chorion SEM analysis, 48 hpf zebrafish embryos were randomly selected from the control, reference Ag-NP (25 mg L^{-1}) and Ag-HEC NP (5 mg L^{-1}) groups (n = 6 each, 2 embryos/group, 3 biological replicates) and anesthetized with MS-222. The chorions were mechanically separated from the embryos by using tweezers and fixed overnight (O/N) in 2% glutaraldehyde in 0.1 M Na-cacodylate buffer (CAC), washed with 0.1 M CAC and post-fixed with 1% osmium tetroxide prepared in 0.1 M CAC for 90 min at room temperature (RT). Each sample was dehydrated with a graded ethanol series up to 100%, infiltrated with hexamethyldisilazane and then left to dry O/N at RT. The samples were placed on SEM aluminium stubs covered with adhesive carbon foil and dried at RT for 2 h under vacuum. In order to increase the conductivity, a 10 nm gold layer was sputtered onto the chorion samples by using high vacuum Quorum Q 159T-ES systems. Afterwards, the chorion morphology and the presence of Ag-NPs over the chorion surface were analyzed through SEM (Zeiss Gemini 500 FEG SEM) coupled with energy-dispersive X-ray spectroscopy (SEM-EDX). SEM micrographs were acquired with an accelerating voltage of 10 kV and a working distance (WD) of 10 mm.

2.7. Whole-mount staining

To improve optical transparency of zebrafish embryos in whole mount staining, the embryos were treated shortly before 24 hpf with 75 μM 1-phenyl 2-thiourea (PTU) that inhibits melanogenesis.[33] At the end of the FET test (96 hpf), the control and malformed treated larvae (25 mg L^{-1} Ag-NKD, 10 mg L^{-1} Ag-PVP, 5 mg L^{-1} Ag-HECs, 1 mg L^{-1} Ag-HECp) (n = 5 larvae for each experimental group, 3 biological replicates) were randomly divided into two groups. One group (96 hpf) was immediately anesthetized in MS-222 0.016% before fixation. The other was maintained in FET solution and processed at 120 hpf to track for an additional 24 h the development of the two selected endpoints.

To monitor yolk lipid retention, whole mount Oil Red O (ORO) staining was performed accordingly to Cornet *et al.* with minor modification.[34] Briefly, 96 and 120 hpf larvae were fixed in 4% paraformaldehyde for 2–4 h at RT, washed 3 times with PBS and submerged twice for 10 min in propylene glycol (PG) at 85% and 100%, respectively. Staining was achieved with 0.5% ORO in 100% PG O/N at RT with gentle rocking, followed by washing in 100% PG for 30 min, 85% PG for 50 min and 85% PG + equal volume of PBS for 40 min. After final washing in PBS, the larvae were observed under a dissecting microscope (Zeiss, Germany) equipped with digitising software AxioVision.

To clearly observe the cartilage structures, 96 and 120 hpf larvae were stained with the selective dye Alcian blue, which binds to the typical sulfur-containing glycosaminoglycans of the cartilaginous matrix. Anesthetized larvae were fixed in 10% buffered formalin O/N at RT and stained O/N at 4 °C with 0.01% Alcian blue 8GX in 70% ethanol and then cleared in a mixture of benzyl alcohol : 70% ethanol : glycerine (1 : 2 : 2).[35] Each cartilage-stained larva was embedded in 3% methyl cellulose in the correct orientation (ventral position and left lateral position) and photographed with the Zeiss microscope mentioned above for qualitative and quantitative assessment with Zen 3.4 software. The following pharyngeal cartilages' angles were evaluated: Meckel's–Meckel's (M–M) angle, ceratohyal–palatoquadral cartilage (CH–PQ) angle, CH–CH angle, PQ–Meckel's angle.

2.8. Statistical analyses

All data were expressed as means ± standard error (SE). Data were tested for homogeneity (Shapiro–Wilk test) and equality of variances (Brown–Forsythe test), and statistically significant differences between experimental groups in mortality, malformed embryos, hatching rates and morphological measurements were detected at p values $<$ 0.05 by one-way analysis of variance (ANOVA) followed by the Bonferroni and Fisher LSD *post hoc* test. Percentages of each single abnormal phenotype were investigated by the chi-square method, using Yates's correction for continuity (χ^2test) or Fisher's exact tests. The elaboration of mortality percentages, malformed embryo percentages and cumulative hatching data of zebrafish embryos by probit analysis[36] allowed obtaining the 96 hpf median lethal concentration (LC_{50}), median effective concentration (EC_{50}) and median hatching time (HT_{50}) values, respectively. Teratogenicity for each compound was calculated as the teratogenic index (TI), *i.e.*, the ratio between LC_{50} and EC_{50} for each Ag-NP. All statistical tests were applied with at least 95% confidence interval using the IBM SPSS statistic 28 software.

Correlation analysis among physical and chemical parameters and biological outcomes was performed using R (R Core Team 2022). Significant correlations were considered at p values $<$ 0.05. Correlations between p-chem and biological outcomes and correlations among the biological outcomes were specifically investigated for identifying NP properties that may determine the observed biological effects and to explore the likelihood of association between different biological outcomes. These latter associations may in fact be predictors of relevant altered biological processes. The Pearson coefficients, evaluated with the Hmisc package,[37] are reported with statistical significance.

3. Results

3.1. Characterization of Ag-NP suspensions

To support the interpretation of biological test results, the main physical characteristics of the benchmark and newly synthesized Ag-NPs such as shape, primary size, mean hydrodynamic diameter, dispersibility and ζ potential *vs.* time of exposure in DI water and FET solution were investigated (Fig. 1). For all Ag-NPs, TEM images showed spherical primary particles that formed heterogeneous agglomerates, hundreds of nm large in the case of Ag-NKD and Ag-PVP and well dispersed for the HEC doped Ag-NPs with a narrow size distribution of 3–20 nm for Ag-HECs and 5–50 nm for Ag-HECp, as reported in previous studies.[30]

DLS analysis of the Ag-NPs in DI water and FET solution was performed at three time points (t0, t24, t96 h) to cover the entire duration of the FET test, at the concentrations selected on the embryotoxicity result basis (10 and 100 mg L^{-1} for reference Ag-NPs and 10 mg L^{-1} for the novel ones) (Fig. 1E). As expected, particularly for Ag-HEC based materials, the hydrodynamic diameter (D_h) is larger compared to that measured by TEM, because of the polymer shell involving a massive steric hindrance. For Ag-NKD and Ag-PVP NPs, the large D_h values are consistent with the formation of aggregates in suspension, typical of nanopowders prepared by high temperature processes. The differences in the size and ζ potential between DI water and the test medium were not significant. The D_h of all Ag-NPs decreased over 24 h in both DI water and FET solution probably due to some precipitation phenomena subtracting larger particles from the detector and then remained almost unchanged up to 96 h when the NPs were dispersed in DI water. Only HEC coated Ag-NPs showed a significant decrease of D_h, when moving from DI water to FET solution. ζ potential values at t0 were negative (ranging from −6 and −21

mV) for Ag-NKD and Ag-PVP NPs, while those of Ag-HEC coated NPs were positive; for all NPs, the ζ potential values remained essentially unchanged at 24 h and 96 h (data not shown). The Z potential measured in FET solution pointed out lower absolute values than in DI, typical of reduced electrosteric colloidal stability. This behaviour is consistent

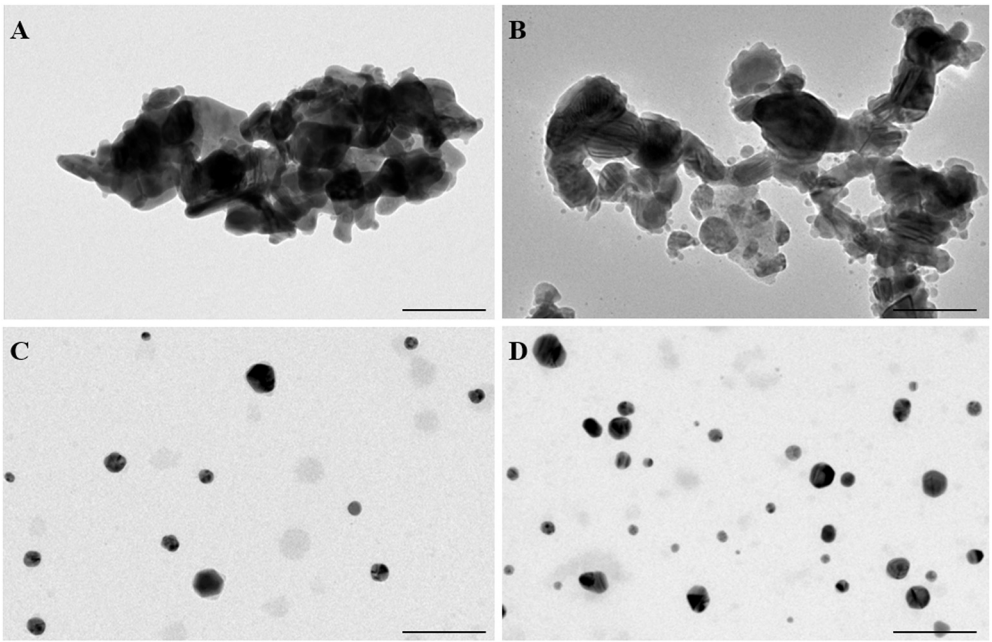

E

Ag-NPs mg/L	Primary size [a] (nm)	Medium	Hydrodynamic size, nm (PdI) [b] 0 h	24 h	96 h	ζ- potential 0 h
Ag-NKD 10	<150nm	DI	317 ± 104 (0.61 ± 0.06)	113 ± 70 (0.51 ± 0.08)	117 ± 89 (0.45 ± 0.06)	−13 ± 17
		FET	340 ± 203 (0.63 ± 0.15)	162 ± 51 (0.51 ± 0.09)	216 ± 61 (0.51 ± 0.04)	− 6 ± 9
Ag-NKD 100		DI	302 ± 114 (0.38 ± 0.02)	71 ± 32 (0.48 ± 0.11)	95 ± 71 (0.52 ± 0.06)	− 21 ± 1
		FET	260 ± 145 (0.42 ± 0.02)	82 ± 17 (0.39 ± 0.11)	64 ± 7 (0.45 ± 0.07)	− 17 ± 3
Ag-PVP 10	<100 nm	DI	254 ± 102 (0.64 ± 0.05)	112 ± 17 (0.45 ± 0.09)	102 ± 37 (0.35 ± 0.01)	− 20 ± 2
		FET	343 ± 209 (0.72 ± 0.16)	186 ± 50 (0.52 ± 0.05)	307 ± 137 (0.65 ± 0.04)	− 10 ± 1
Ag-PVP 100		DI	243 ± 15 (0.56 ± 0.04)	90 ± 12 (0.39 ± 0.05)	67 ± 14 (0.49 ± 0.17)	− 17 ± 1
		FET	193 ± 99 (0.59 ± 0.06)	96 ± 23 (0.40 ± 0.07)	88 ± 24 (0.45 ± 0.09)	− 10 ± 1
Ag-HECs 10	3-20 nm	DI	119 ± 3.00 (0.16 ± 0.02)	102 ± 6 (0.17 ± 0.03)	90 ± 3 (0.18 ± 0.01)	− 13 ± 2
		FET	89 ± 5 (0.18 ± 0.00)	80 ± 4 (0.18 ± 0.01)	77 ± 2 (0.18 ± 0.03)	− 4 ± 4
Ag-HECp 10	5-50 nm	DI	372 ± 7.00 (0.34 ± 0.03)	244 ± 14 (0.39 ± 0.02)	186 ± 33 (0.45 ± 0.07)	17 ± 1
		FET	280 ± 37 (0.33 ± 0.03)	80 ± 4 (0.29 ± 0.01)	225 ± 18 (0.30 ± 0.02)	9 ± 1

[a] *TEM data;* [b] *PdI: polydispersity index.*
data are represented as mean ± SD

Fig. 1 Physico-chemical properties of the Ag-NPs. (A–D) Transmission electron microscopy (TEM) images of Ag-NKD (A), Ag-PVP (B), Ag-HECs (C) and Ag-HECp (D). (E) Hydrodynamic diameter and ζ potential by dynamic and electrophoretic light scattering. The average size and standard deviation were calculated using the maximum peak values for each hydrodynamic and ζ-potential measurements from triplicate trials for each suspension. Data are represented as mean ± SD. FET: embryo rearing solution; DI: distilled water. Scale bar = 100 nm.

with the DLVO model and is due to the high ionic strength of the FET solution triggering the shrinkage of the electric double layer.

As reported in ESI† Table S1, no significant release of Ag occurred when dispersing Ag-NPs in FET solution, the detected Ag values were often close to the instrumental LOD (>0.01 mg L^{-1}). The very low concentration of Ag ions detected for all NPs could be due to the high chloride content in the FET medium itself, which most likely complexed with and precipitated the Ag^{+} ions, making them no longer available for detection.

3.2. Ag-NP embryotoxicity

The Ag-NP embryotoxicity was evaluated by monitoring embryos daily during the FET test to determine the mortality and malformed embryo rates, time of hatching and specific malformation prevalence.

Zebrafish embryos exposed to all tested Ag-NPs developed concentration-dependent lethal and sub-lethal effects (Fig. 2).

However, the embryotoxic effects occurred at lower concentrations in embryos exposed to the HEC coated Ag-NPs than in those exposed to the reference NPs, with a significant incidence of dead and malformed embryos starting from 5 mg L^{-1} for Ag-HECs and 1 mg L^{-1} for Ag-HECp against the 25 mg L^{-1} for Ag-NKD and Ag-PVP. On the other hand, HEC alone was demonstrated to be safe at the concentrations (1 and 10 mg L^{-1}) at which the Ag-HEC NPs showed significant embryotoxicity (ESI† Fig. S1).

The acute embryotoxicity was particularly evident for Ag-HECp NPs as, at the exposure concentration greater than 1 mg L^{-1}, most of the mortality occurred very early (within 24 hpf). In contrast, for the other Ag-NPs there was a gradual increase of mortality over 96 h of exposure for all concentrations tested (ESI† Fig. S2).

The 96 hpf-LC_{50} and EC_{50} values extrapolated from the concentration–response curves related to the mortality and malformed embryo rates confirmed the higher toxicity of Ag-HEC NPs compared to the reference ones (Table 1). The absence of confidence intervals' overlap between the reference and Ag-HEC NPs suggested a statistical difference in 96 hpf-LC_{50} and EC_{50} values. Ag-HECp was 1.95–2.6 times more toxic than Ag-HECs, but comparing the confidence intervals, this difference in toxicity cannot be considered statistically significant.

Finally, all Ag-NPs tested were not classifiable as teratogens in zebrafish having a TI < 3.[38] The substantial embryotoxicity rather than teratogenicity of Ag-NPs is also supported by the strong positive correlation between mortality and malformed embryo rates (see Fig. 7).

Regarding hatching ability, which is known to be often impaired in zebrafish embryos exposed to metal-based NPs,

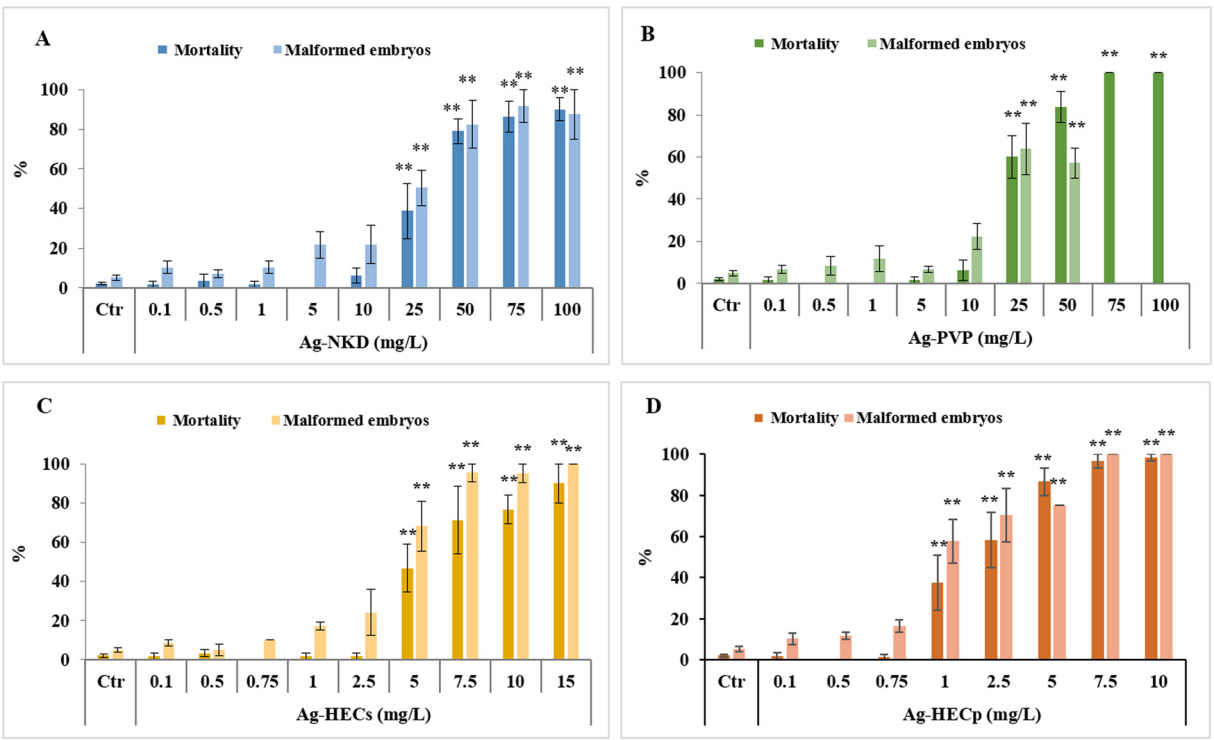

Fig. 2 Embryotoxicity of Ag-NPs evaluated by FET. Mortality and malformation rates in 96 hpf zebrafish embryos after exposure to naked (A) and polyvinylpyrrolidone (PVP) coated (B) Ag-NPs (0.1–100 mg L^{-1}) and to hydroxyethyl cellulose embedded Ag-NP suspension (HECs) (C) and powder (HECp) (D) (0.1–10 mg L^{-1}). All values in the graphs are given as mean ± SE of at least three independent assays. *$p < 0.05$, **$p < 0.01$ indicate statistical difference from the control; #$p < 0.05$, ##$p < 0.01$ indicate statistical difference between Ag-HEC NPs and reference NPs; °$p < 0.05$, °°$p < 0.01$ indicate statistical difference between Ag-HECs and Ag-HECp NPs (ANOVA + *post hoc* Bonferroni).

Table 1 Median lethal concentration (96 hpf, LC_{50}), median effective concentration (96 hpf, EC_{50}) and teratogenic index (TI) after exposure of zebrafish embryos to Ag-NPs

	Ag-NKD	Ag-PVP	Ag-HECs	Ag-HECp
96 hpf-LC_{50} (mg L^{-1})	**44.29** (32.81–60.88)	**30.45** (25.34–37.33)	**6.84**[a] (5.28–9.23)	**2.91**[a] (1.41–10.89)
96 hpf-EC_{50} (mg L^{-1})	**40.03** (26.59–79.84)	**31.80** (21.59–62.56)	**4.68**[a] (4.15–5.37)	**2.12**[a] (1.45–4.67)
TI (LC_{50}/EC_{50})	**1.11**	**0.96**	**1.46**	**1.37**

Note: confidence intervals 5–95% are indicated in the brackets. [a] Statistically different from Ag-NKD and Ag-PVP NPs based on the confidence interval comparison.

Ag-HEC NPs were found to interfere more than the reference Ag-NPs with this process as well, which is particularly remarkable considering the lower concentration range used.

Interestingly, based on HT_{50} extrapolated from cumulative hatching rates (ESI† Fig. S3), Ag-HECs showed a slight tendency to anticipate the hatching process as concentrations increased (Table 2).

Conversely, Ag-HECp exhibited an opposite trend, causing delayed hatching at the higher concentrations tested. However, at 96 hpf no significant change in the hatching rate was observed regardless of treatment, except for 1 and 2.5 mg L^{-1} Ag-HECp, which inhibited hatching in approximately 40% of embryos (ESI† Fig. S3). However, considering Pearson coefficients, a low (−0.33) but significant negative correlation between malformed embryos and hatching rates at 96 hpf was evidenced, suggesting that malformed phenotypes negatively impact hatchability considering the whole set of NPs tested (see Fig. 7).

Observing the embryos under the stereomicroscope during the FET test, agglomerates of particles adhering to the external surface of the chorion were highlighted (Fig. 3, column 1 LM), therefore a SEM analysis was applied to explore if the chorion structure was affected by Ag-NP interaction. The outer and inner layers (OL and IL respectively) of the control group's chorion appeared to have a smooth surface with delineated, uniformly sized, and visibly open pores (Fig. 3, column 1 OL, column 2 IL). Exposed embryos' chorions revealed instead a rough surface on both sides with deformed plugs on the OL and irregular, enlarged and partially blocked pores on the IL (Fig. 3, column 1, OL).

Ag-NKD and Ag-HEC NPs were detected on the inner surface of the chorion by EDX mapping, which confirmed Ag identity, indicating the possible random passage of the smallest Ag-NPs through the chorion pores (ESI† Fig. S4).

However, sub-lethal exposure to all Ag-NPs did not lead to a detectable increase in total Ag concentrations in 96 hpf zebrafish larvae compared to the controls, likely due to Ag values very close to the ICP-OES instrumental LOD and the presence of a background Ag concentration in the controls (ESI† Fig. S5).

3.3. Developmental adverse effects

The comparative toxicity profile of the novel and benchmark Ag-NPs was expanded by focusing on the evaluation of sublethal changes in zebrafish development.

Several recurrent morphological defects such as bent and twisted notochord, pericardial edema, craniofacial and eye abnormalities, deformation and edema of the yolk sac were observed in surviving zebrafish larvae at the end of the FET test, with an increasing incidence rate and severity at the higher concentrations tested for each Ag-NP (Table 3, Fig. 4 column 1).

Table 2 Median hatching time (HT_{50}) after exposure of zebrafish embryos to Ag-NPs

	Control	Ag-NKD	Ag-PVP	Ag-HECs	Ag-HECp
mg L^{-1}					
0	72.4 ± 2.1				
0.1		78.2 ± 2.2	78.0 ± 1.1	80.0 ± 3.3	74.0 ± 2.5
0.5		74.7 ± 2.1	76.6 ± 0.2	80.8 ± 7.2	74.8 ± 2.7
0.75				75.4 ± 0.3	80.5 ± 2.4
1		74.9 ± 0.9	72.9 ± 0.1	81.3 ± 3.8	85.4 ± 4.2**
2.5				73.2 ± 1.2	86.0 ± 6.0**
5		77.7 ± 2.9	79.7 ± 1.5	68.5 ± 5.2	79.0 ± 5.6
7.5				59.7 ± 0.8*	88.1*
10		76.5 ± 2.6	77.6 ± 1.3	62.2 ± 1.7*	
15				69.2	
25		73.2 ± 3.2	64.9 ± 0.9*		
50		74.3 ± 4.6	71.1 ± 0.8		
75		79.0 ± 5.0			
100		79.9 ± 4.5			

Note: HT_{50} stands for time, expressed as hpf, required for 50% hatching of embryos. All values are presented as the mean ± standard deviation. *$p < 0.05$, **$p < 0.01$ versus the control group.

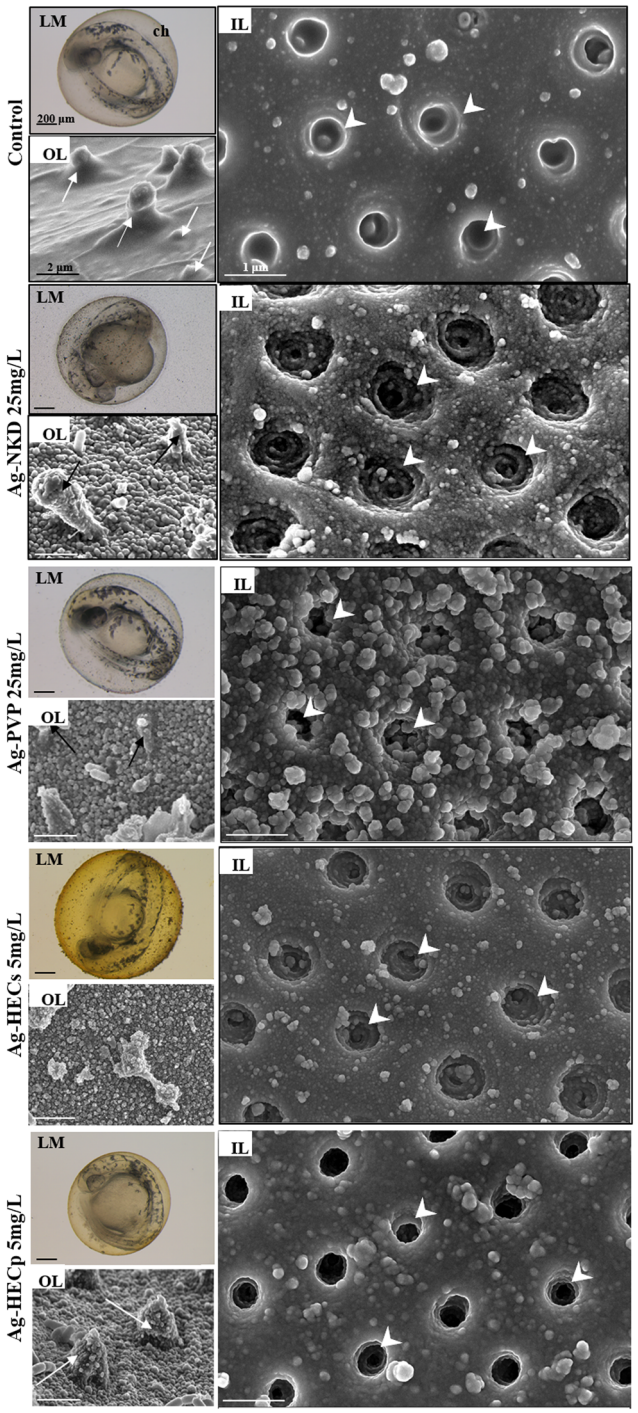

Fig. 3 Light stereomicroscopy (LM) and scanning electron microscopy (SEM) analysis of zebrafish chorions from the control and Ag-NP exposed 48 hpf zebrafish embryos. Column 1: representative LM images of the whole embryo surrounded by the chorion (top) (scale bar = 200 μm) and SEM images of the chorion outer layer (OL, down) (scale bar = 2 μm) of the control and Ag-NP exposed embryos. Column 2: representative SEM images (scale bar = 1 μm) of the chorion inner layer (IL) of the control and Ag-NP exposed embryos. SEM analysis showed the pore plugs on the OL (arrows) and the cone shaped pores on the IL (arrowheads).

Although delayed yolk sac absorption was not considered as a teratogenic endpoint, this phenotypic feature was observed in all Ag-NP exposed groups with a concentration-dependent incidence (ESI† Fig. S6). Furthermore, comparing the two HEC-doped Ag-NPs, Ag-HECp slowed down the yolk absorption already at the lowest concentrations (0.1–0.75 mg L^{-1}) with a statistically significant rate compared to Ag-HECs. The EC_{50} values calculated for each phenotypic feature were higher for the reference NPs than for the newly synthesized ones and revealed that the most sensitive phenotypes were the reduction of yolk absorption, the axis defects and pericardial edema (ESI† Table S2). However, other abnormalities such as absent or aberrant pectoral fins, craniofacial alterations, and general growth retardation were found to occur at low concentrations especially for HEC doped Ag-NPs (ESI† Table S2).

The cross-correlation of all endpoints indicated that they were positively correlated with each other, showing that the occurrence of one abnormal phenotype was associated with the presence of other abnormalities (see Fig. 7).

Reduced yolk absorption and head malformations were observed at exposure concentrations below the LC_{50} values for the different materials. In order to correlate the aberrant yolk sac size with the toxic effects of Ag-NPs on early embryonic nutrition, embryos were stained with the lipophilic dye ORO to highlight the mobilization of neutral lipid constituents of the yolk (Fig. 4, columns 2 and 3).

In the 96 hpf control larvae, ORO stained the yolk sac, head, swim bladder and vessels such as the posterior cardinal vein, dorsal aorta and intersegmental vessels (Fig. 4, column 2). In contrast, larvae exposed to Ag-NPs, particularly those treated with HEC-doped ones, showed stronger ORO staining of the yolk sac and clear reduction in staining of the swim bladder and vasculature. At 120 hpf, a stained yolk sac and a small or uninflated swim bladder remained in the treated larvae compared to the control (Fig. 4, column 3).

Furthermore, to verify if the craniofacial malformations observed at the end of the FET test were related to altered chondrogenesis in the head and jaws, qualitative and quantitative morphometric evaluation on Alcian blue stained 96 and 120 hpf larvae was applied (Fig. 5 and ESI† Fig. S7).

Treatment with Ag-NPs did not appear to have altered chondrogenesis, as the craniofacial cartilaginous elements, *i.e.* Meckel's and palatoquadrate cartilages, which constitute respectively the elements of the lower and upper jaw, the ceratohyal cartilages and the gill basket are recognisable. However, compared to the control, the typical pattern of the craniofacial skeleton in most of the treated larvae (except those of Ag-PVP) was similar to that of an earlier developmental stage.

Quantitative morphometric analysis of Ag-NP effects on the head skeleton was performed by measuring the angles of the visualized cartilaginous structures (ESI† Fig. S7). Except for Ag-PVP, exposure to sublethal concentrations of all other Ag-NPs

Table 3 Pattern of malformations in zebrafish embryos exposed to Ag-NPs

	Ag-NKD (mg L^{-1})																		Ag-PVP (mg L^{-1})													
	Ctr		0.1		0.5		1		5		10		25		50		75		100		0.1		0.5		1		5		10		25		50	
A	*n*	%	*n*	%	*n*	%	*n*	%	*n*	%	*n*	%	*n*	%	*n*	%	*n*	%	*n*	%	*n*	%	*n*	%	*n*	%	*n*	%	*n*	%	*n*	%	*n*	%
Craniofacial malformation							1	1.7	6	10.0^{a}	6	8.0^{b}	12	24.5^{b}	7	33.3^{b}	2	18.2^{b}	1	12.5^{b}	2	3.4					2	3.4	2	2.7	4	16.7^{b}	4	28.6^{b}
Sacculi/otolith malformation			3	5.1^{a}							5	6.7^{b}	6	12.2^{b}	3	14.3^{b}	1	9.1^{b}									1	1.7						
Eye defects	2	0.6	1	1.7			3	5.0^{a}	4	6.7^{a}	5	6.7^{b}	9	18.4^{b}	6	28.6^{b}			1	12.5^{b}	4	6.8^{b}					3	5.1^{a}	1	1.3	4	16.7^{b}		
Heart malformation/edema	12	3.5	4	6.8	3	5.2	3	5.0	10	16.7^{a}	13	17.3^{b}	12	24.5^{b}	7	33.4^{b}	3	27.3^{b}	3	37.5^{b}			8	13.3^{b}	3	5.0	4	6.8	9	12.2^{a}	12	50.0^{b}	7	50.0^{b}
Spinal cord malformation	1	0.3											2	4.1	2	9.5^{b}	1	9.1^{b}	3	37.5^{b}													
Lordosis											1	1.3	5	10.2^{b}	3	14.3^{b}			1	12.5^{b}							1	1.7			3	12.5^{b}		
Kyphosis									2	3.3^{a}	5	6.7^{b}	8	16.3^{b}	4	19.0^{b}	1	9.1^{b}	1	12.5^{b}	1	1.7					3	5.1^{b}	3	4.0^{a}	1	4.2^{a}		
Scoliosis			1	1.7					1	1.7	7	9.3^{b}	9	18.4^{b}	6	28.6^{b}	3	27.3^{b}	3	37.5^{b}	2	3.4^{a}	1	1.7	2	3.3^{a}	6	10.2^{b}			2	8.3^{a}	4	28.6^{b}
Yolk deformation/edema	2	0.6			2	3.4^{a}			1	1.7	3	4.0^{a}	7	14.3^{b}	6	28.6^{b}			1	12.5^{b}	1	1.7	s		2	3.3^{a}	8	13.6^{b}	9	12.2^{b}	9	37.5^{b}	6	42.9^{b}
General growth retardation					1	1.7					4	5.3^{b}	7	14.3^{b}	2	9.5^{b}					1	1.7			1	1.7	2	3.4^{a}						
Short tail					1	1.7					5	6.7^{b}	8	16.3^{b}	4	19.0^{b}	1	9.1^{b}	1	12.5^{b}	1	1.7			1	1.7	2	3.4^{a}			2	8.3^{a}		
Impaired fin development											6	8.0^{b}	15	30.6^{b}	8	38.1^{b}	5	45.4^{b}	6	75.0^{b}							2	3.4^{a}						
Living embryos 96 hpf (*n*)	**339**		**59**		**58**		**60**		**60**		**75**		**49**		**21**		**11**		**8**		**59**		**60**		**60**		**59**		**74**		**24**		**14**	

	Ag-HECs (mg L^{-1})																Ag-HECp (mg L^{-1})															
	0.1		0.5		0.75		1		2.5		5		7.5		10		15		0.1		0.5		0.75		1		2.5		5		7.5		10	
B	*n*	%	*n*	%	*n*	%	*n*	%	*n*	%	*n*	%	*n*	%	*n*	%	*n*	%	*n*	%	*n*	%	*n*	%	*n*	%	*n*	%	*n*	%	*n*	%	*n*	%
Craniofacial malformation							5	8.5^{b}			20	31.3^{b}	12	52.2^{b}	7	50.0^{b}	4	66.7^{b}					1	1.3	16	16.0^{b}	20	40.0^{b}	2	25.0^{b}	2	100.0^{b}		
Sacculi/otolith malformation											8	12.5^{a}	2	8.7^{a}	3	21.4^{b}	5	83.3^{b}							5	5.0	7	14.0^{b}						
Eye defects	1	1.7					1	1.7			15	23.4^{b}	9	39.1^{b}	4	28.6^{b}	3	50.0^{b}					2	2.5	11	11.0^{b}	17	34.0^{b}	1	12.5^{a}				
Heart malformation/edema	2	3.4	3	5.2	5	8.3	8	13.6^{a}	12	20.3^{b}	20	31.3^{b}	13	56.5^{b}	10	71.4^{b}	5	83.3^{b}	7	11.9^{b}	6	10.0^{a}	11	13.9^{a}	13	13.0^{b}	26	52.0^{b}	4	50.0^{b}	1	50.0^{b}		
Spinal cord malformation															1	7.1^{a}							1	1.3										
Lordosis	1	1.7									1	1.6	1	4.3^{a}													1	2.0			1	50.0^{b}		
Kyphosis	1	1.7									24	37.5^{b}	14	60.9^{b}	6	42.9^{b}	2	33.3^{b}					1	1.3	13	13.0^{b}	5	10.0^{b}	4	50.0^{b}				
Scoliosis			1	1.7			2	3.4^{a}			11	17.2^{b}	6	26.1^{b}	3	21.4^{b}	1	16.7^{b}			1	1.7	4	5.1^{b}	11	11.0^{b}	15	30.0^{b}			1	50.0^{b}	1	100.0^{b}
Yolk deformation/edema			1	1.7	1	1.7	4	6.8^{b}		13.6^{b}	15	23.4^{b}	14	60.9^{b}	6	42.9^{b}	6	100^{b}	4	6.8^{b}			14	17.7^{b}	22	22.0^{b}	15	30.0^{b}	3	37.5^{b}	2	100.0^{b}		
General growth retardation							2	3.4^{a}			21	32.8^{b}	3	13.0^{b}	8	57.1^{b}	3	50.0^{b}							13	13^{b}	14	28.0^{b}	2	25.0^{b}			1	100.0^{b}
Short tail							1	1.7			2	3.1^{a}	1	4.3^{a}	8	57.1^{b}	4	66.7^{b}					1	1.3	11	11.0^{b}	3	60^{a}						
Impaired fin development											17	26.6^{b}	13	56.5^{b}	3	21.4^{b}							2	2.5^{a}	10	10.0^{b}	8	16.0^{b}						
Living embryos 96 hpf (n)	**59**		**58**		**60**		**59**		**59**		**64**		**23**		**14**		**6**		**59**		**60**		**79**		**100**		**50**		**8**		**2**		**1**	

Percentages are based on the number of malformations/number of those living. ^{a} $p < 0.05$. ^{b} $p < 0.001$ *vs.* control (chi square test)

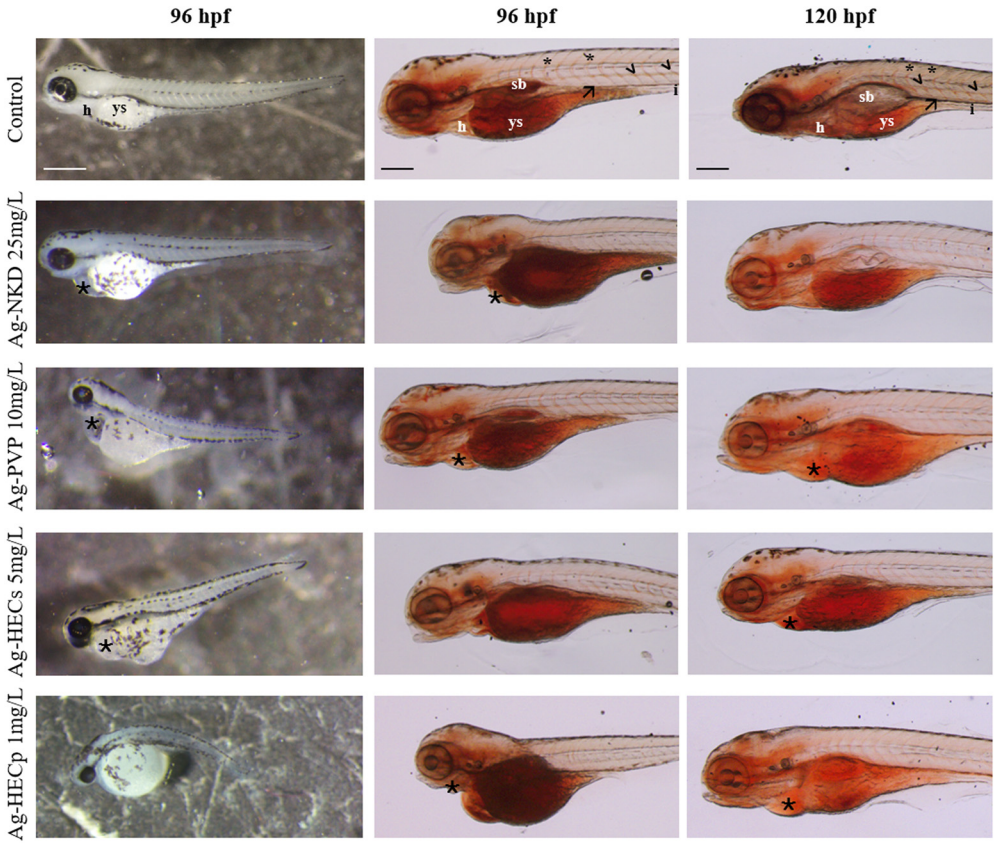

Fig. 4 Analysis of the yolk lipid content. Stereomicroscopic lateral view of the control and Ag-NP exposed larvae at 96 hpf and 120 hpf. Column 1: representative phenotypic alterations at the end of the FET test. Columns 2 and 3: whole-mount Oil Red O staining of randomly selected larvae of the control and Ag-NP groups. ORO staining indicates the content and distribution of neutral lipids in the larvae. Ag-NPs impair endotrophic lipid consumption during zebrafish development. Scale bar column 1 = 500 μm; scale bar columns 2 and 3 = 200 μm. Abbreviations: h: heart; ys: yolk sac; sb: swim bladder; (☆): cardiac oedema; (*): intersegmental vessel; (<): dorsal artery; (→): posterior cardinal vein.

resulted in a significant increase of the M–M and CH–CH angles in the 96 hpf larvae, a change that also extends to the M–PQ and PQ–CH angles in the 120 hpf larvae.

3.4. Morphometric analyses

The qualitative phenotypic analyses of Ag-NP induced defects for each larva were integrated by quantitative data derived from morphometric characteristics (Fig. 6), which are very sensitive parameters detectable at sub-teratogenic concentrations (*i.e.* at concentrations at which no malformations are observed in embryos).

The results showed that groups exposed to Ag-NPs differed significantly from the controls for morphological parameters related to embryo growth (body length and yolk sac area) starting from 10–25 mg L^{-1} for Ag-NKD and Ag-PVP and 0.5–1 mg L^{-1} for Ag-HECs and Ag-HECp (Fig. 6A and B). A statistically significant decrease in body length and an increase in yolk sac area were observed among all NPs tested and confirmed by the negative Pearson coefficient (Fig. 7).

Morphometric measurements showed that all tested Ag-NPs significantly affected also the skeletal (head width) and sensorial (eye area and diameters) parameters. However, the stunted growth of embryos was allometric as bivariate analysis showed a strong positive correlation between the larva length and head width and/or eye size (Fig. 7).

Interestingly, all quantitative measurements (body length, head size and eye size) showed a negative correlation with all other altered phenotypes (Fig. 7).

3.5. Correlation between NP properties and adverse effects

The understanding of the material properties that mostly affected the reported effects was explored by analysing the overall correlations between the biological outcomes and the NP p-chem properties (Table 4).

The main adverse outcomes, such as lethality and total malformed embryos, showed a significant correlation with the concentration of exposure (0.60 and 0.50, respectively). Interestingly a positive association of these outcomes was observed also with the total dissolved ions measured at 24 h (0.43 and 0.37 for mortality and total malformations, respectively) and at 96 h (0.53 and 0.48 for mortality and total malformations, respectively), suggesting therefore that besides the particles, ions can also play a role in the toxicity

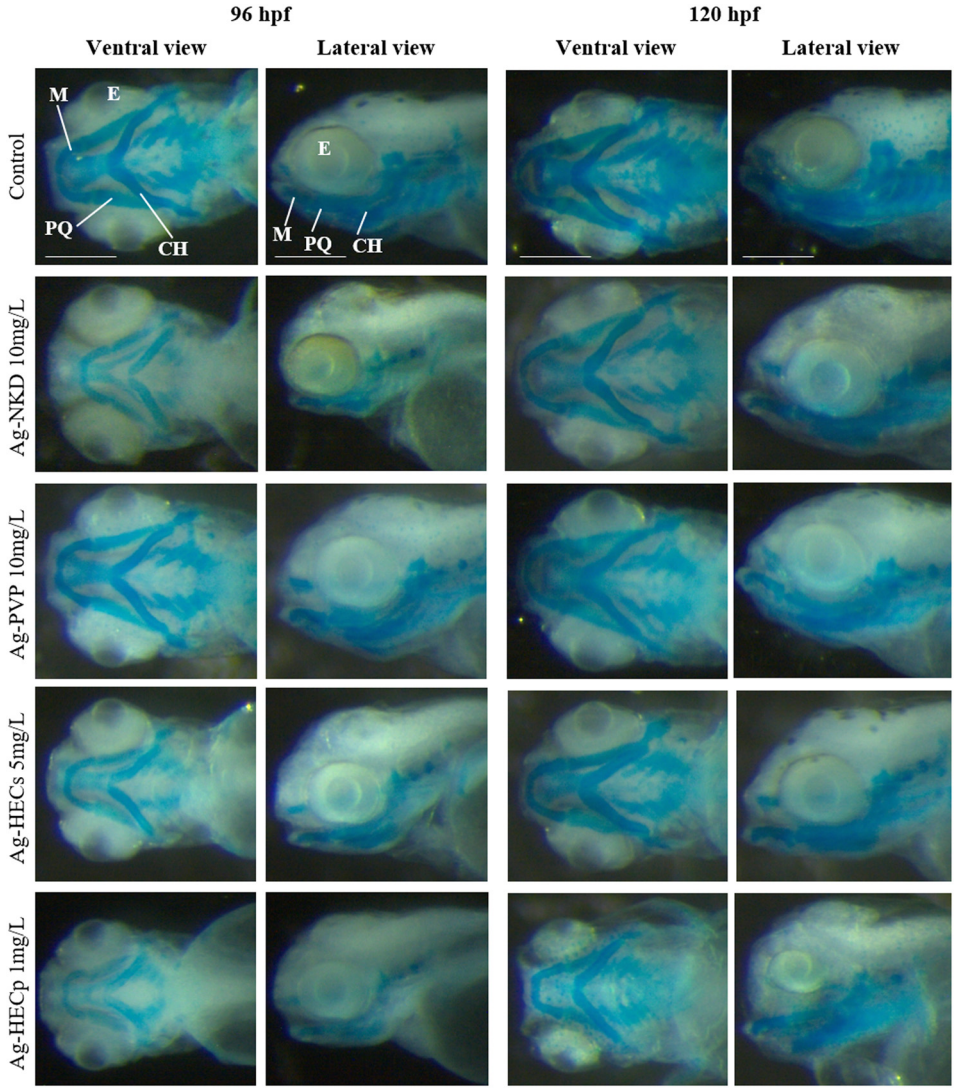

Fig. 5 Analysis of craniofacial cartilages. Stereomicroscopic ventral and lateral view of the control and Ag-NP exposed zebrafish embryos at 96 and 120 hpf. Whole-mount Alcian blue staining showing the cartilage morphology of the head and branchial region. In all images, the rostral region is to the left. All embryos are shown at the same scale (scale bar = 200 μm). Abbreviations: M = Meckel's cartilage; CH = ceratohyal cartilage; PQ = palatoquadrate; E = eye.

of the tested NPs. The correlation with the dissolved ions should, however, be considered with caution, taking into account the limitations already described for our data. The exposure concentration also showed a significant positive correlation with specific altered phenotypes, such as spinal cord malformations (0.51), reduced yolk resorption (0.33) and impaired fin development (0.44). Interestingly, the spinal cord malformations and impaired fin development showed a significant correlation with the dissolved ions measured at 24 h (Pearson coefficients of 0.52 and 0.44, respectively) and at 96 h (Pearson coefficients of 0.53 and 0.46, respectively). The correlation reported confirmed the observation that some of the NPs tested determined specific outcomes. Yolk defects were mostly correlated with the Ag-HEC particles as indicated by the positive association for the yolk area (0.31) and reduced yolk resorption (0.56) with the variable "group" (Table 4). Again, this correlation should, however, be taken with caution. The number of different NPs tested here, which is only four, may introduce bias in the reported correlations. In the future, it would be desirable to have a broader dataset with a greater number of different NPs, ideally more than 10, tested under similar conditions. Among the other analysed physical variables, noteworthy is the negative correlation between the ζ-potential and the hatching at 96 h. The negative sign in the correlation indicates that positive ζ-potentials are related to a reduction of the hatching observed at 96 h. This correlation, although affected by the specific outcomes observed for the Ag-HEC doped NPs, suggests that also in the zebrafish model, the ζ-potential may provide information on specific sub-lethal endpoints and should be further explored.

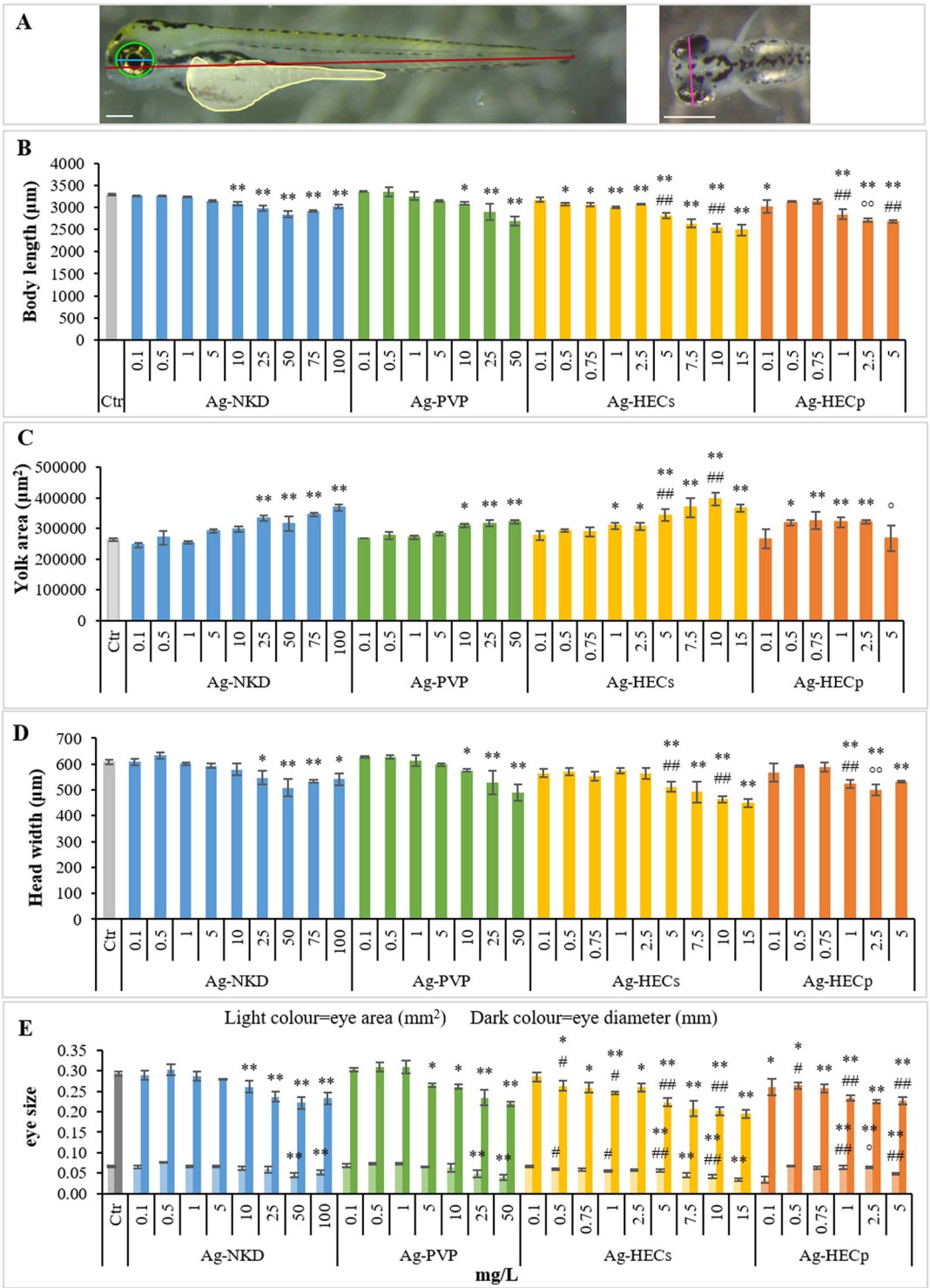

Fig. 6 Morphometric parameters of the control and exposed zebrafish embryos. A) Description of morphological traits measured from the lateral (left) and dorsal (right) images of the 96 hpf control embryo. Measured traits are as follows: body length (red), yolk sac area (yellow), eye area (green), eye diameter (blue) and head width (orange). Lateral view, scale bar 200 µm; dorsal view, scale bar 500 µm. B–E). All values in the graphs are given as mean ± SE of at least three independent assays. *$p < 0.05$, **$p < 0.01$ indicate statistical difference from the control; #$p < 0.05$, ##$p < 0.01$ indicate statistical difference between Ag-HEC NPs and reference NPs; °$p < 0.05$, °°$p < 0.01$ indicate statistical difference between Ag-HECs and Ag-HECp NPs (ANOVA + Fisher LSD method).

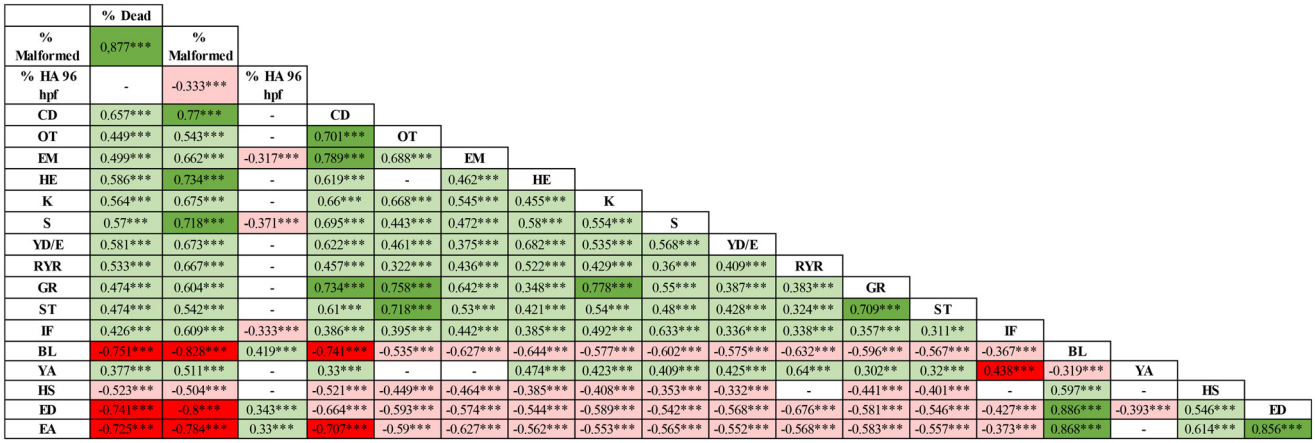

Fig. 7 Pearson correlation matrix between the altered phenotypes evaluated after Ag-NP exposure. Numbers show the degree of correlation between each pair of malformations. The positive correlation is highlighted in green (*i.e.* malformations that occur simultaneously), while the negative correlation by the red color (*i.e.* phenotypes that manifest in the opposite direction). Color intensity is related to the degree of correlation. $^{**}p < 0.01$, $^{***}p < 0.001$. HA = hatching, CD = craniofacial defects, OT = otolith defects, EM = eye malformations, HE = hearth edema, L = lordosis, K = kyphosis, S = scoliosis, YD/E = yolk deformation/edema, RYR = reduced yolk resorption, GR = general growth retardation, ST = short tail, IF = impaired fin, BL = body length, YA = yolk area, HS = head size, ED = eye diameter, EA = eye area.

Table 4 Correlations between biological outcomes and the Ag-NP p-chem properties

	Group	Conc	Primary size	z-ave t0	PdI t0	z-pot t0	z-ave t24	PdI t24	z-ave t96	PdI t96	Bioav_ions t0	Bioav_ions t24	Bioav_ions t96
% Dead	—	0.604 ***	—	—	—	—	—	—	—	—	—	0.433 ***	0.53 ***
% Malformed	—	0.503 ***	—	—	—	—	—	—	—	—	—	0.367 ***	0.481 ***
% HA 96 hpf	−0.381 ***	—	—	—	—	−0.207 ***	—	—	—	—	—	—	—
HT_{50}	—	—	—	—	—	—	—	—	—	—	—	—	—
CD	—	—	—	—	—	—	—	—	—	—	—	—	—
OT	—	—	—	—	—	—	—	—	—	—	—	—	—
EM	—	—	—	—	—	—	—	—	—	—	—	—	—
HE	—	0.313 ***	—	—	—	—	—	—	—	—	0.331 ***	—	—
SP	—	0.507 ***	—	—	—	—	—	—	—	—	—	0.525 ***	0.533 ***
L	—	0.306 **	—	—	—	—	—	—	—	—	—	—	—
K	—	—	—	—	—	219***	—	—	—	—	—	—	—
S	—	0.361 ***	—	—	—	—	—	—	—	—	—	—	0.335 ***
YD/E	—	—	—	—	—	—	—	—	—	—	0.319 ***	—	—
RYR	0.556 ***	0.326 ***	—	—	—	—	—	—	—	—	—	—	0.326 ***
GR	—	—	—	—	—	—	—	—	—	—	—	—	—
ST	—	—	—	—	—	—	—	—	—	—	0.377 ***		—
IF	—	0.437 ***	—	—	—	—	—	—	—	—	—	0.443 ***	0.463 ***
BL	−0.456 ***	—	—	—	—	—	—	—	—	—	—	—	—
YA	0.31 **	—	—	—	—	—	—	—	—	—	—	—	0.325 ***
HS	—	—	—	—	—	—	—	—	—	—	—	—	—
ED	−0.404 ***	−0.382***	—	—	—	−0.233***	—	—	—	—	—	—	−0.319 ***
EA	−0.356 ***	−0.318 ***	—	—	—	−0.256***	—	—	—	—	—	—	—

CD = craniofacial defects, OT = otolith defects, EM = eye malformations, HE = hearth edema, SP = spinal cord, L = lordosis, K = kyphosis, S = scoliosis. YD/E = yolk deformation/edema, RYR = reduced yolk resorption, GR = general growth retardation, ST = short tail, IF = impaired fin, BL = body length. YA = yolk area, HS = head size, ED = eye diameter, EA = eye area. Bioav_ions refers to the amount of Ag^{+} measured with ICP-OES in the FET solution.

4. Discussion

The primary goal of the SbD approach is to assess and enhance safety in the development of NMs or NEPs starting from the early stages of production. This involves addressing environmental impact, technical-economic performance, functionality, and safety throughout the entire life cycle of the product, with the aim of minimizing or eliminating any

unwanted or unexpected risks to human and environmental health. However, the management of safety issues in NM development and the selection of the optimal SbD solution are still areas of ongoing research.

The manipulation of metal-based NMs with antimicrobial properties has been proposed as a valuable and customizable strategy to effectively reduce bacterial infections while minimizing side effects in non-target organisms.

In the EU Horizon 2020 ASINA project, a SbD approach was employed to develop effective antimicrobial Ag-NPs using an environmentally friendly and easily scalable synthetic method.[24] This involved incorporating Ag-based NPs into the eco-friendly biopolymer HEC as a stabilizer and reducing agent. The resulting HEC-coated Ag-NPs were investigated for their selectivity, demonstrating a very high and promising selectivity index in terms of their activity against microbes *versus* human cell toxicity.[24] Nevertheless, our study emphasizes the importance of conducting a comprehensive hazard assessment using whole organisms as experimental models to refine the SbD process and facilitate the commercial utilization of Ag-NPs. This consideration is crucial due to the known toxicity of silver to organisms, even at low concentrations.[39–42] At the same time, Ag-HECs are also a more powerful antibacterial and antiviral agent. In this sense, the SbD applied to biocidal nanomaterials would take into account an accurate balance between the effectiveness and the safety profile of new antimicrobials.

To meet the 3Rs,[43] the Ag-HEC NP potential toxicity was investigated on zebrafish embryos, because before exogenous feeding (up to 120 hpf), they are considered complementary and alternative vertebrate models bridging the simplicity of *in vitro* cell culture to the complexity of *in vivo* mammalian models.[31,44] In addition, zebrafish also allow a focus on aquatic organisms, as surface waters and sediments are the release compartments of Ag-NPs from many used products whose measured concentrations range from 0 to 1700 ng L^{-1} in effluents of wastewater treatment plants and 0.3–8.6 ng L^{-1} in surface freshwater.[45,46]

A first set of experiments was performed according to the standard OECD n. 236 fish embryo toxicity test,[27] useful for generating comparable results that can be adopted for the evaluation of NM toxicity. From literature data, Ag-NPs vary in their toxicological properties in different fish species, mostly due to extensive variations in size, charge, coating, agglomeration, and dissolution of Ag^{+}.[47,48]

However, comparing the toxicological profiles of the various Ag-NPs studied in zebrafish embryos over the years is challenging due to differences in experimental conditions, such as the developmental stage and treatment duration. This hinders the understanding of how variations in Ag-NPs' p-chem properties can drive their toxicity.

In this study, we chose to compare the effects of the two SbD newly developed Ag-NPs coated with HEC in suspension and the powder form, and commercial naked and PVP coated Ag-NPs used here as reference materials. The FET results, also supported by the Pearson correlation analysis, showed a strong concentration-dependent response in terms of mortality and malformed embryos with 96 hpf-LC_{50} and EC_{50} calculated values very close to each other and a consequent TI < 3, indicating more embryotoxicity than teratogenicity for all the tested Ag-NPs.[38] Unexpectedly, based on these values, Ag-HEC NPs were four to fifteen times more toxic than the reference NPs with 96 hpf-LC_{50} of 6.84 mg L^{-1} for Ag-HECs and 2.91 mg L^{-1} for Ag-HECp. Since HEC alone was non-toxic at the concentration of Ag-HEC treatment suspensions causing near 100% mortality, the increased toxicity of Ag-HEC NPs could be attributed to the specific p-chem properties dictated by such surface coating as the higher the stability, the lower the agglomeration in FET medium and the smaller the DLS hydrodynamic size, in comparison with the reference Ag-NPs. However, these p-chem properties did not correlate with the adverse outcomes, meaning that HEC may have played a role in facilitating Ag-NP biointeraction with the chorion before hatching and subsequently with larvae, where the NPs exerted their toxicity. In a study on cancer therapy, this polymer has indeed been shown to promote the internalization of methotrexate in cancer cells and thus be used successfully as a drug carrier.[48] Comparing the two novel NPs, Ag-HEC in the powder form displayed the highest toxicity in zebrafish embryos, as already observed in the AOP oriented study on an alveolar *in vitro* model, A549 cells, by Motta and collaborators.[30] As suggested in the mentioned paper, the possible p-chem transformations of the coating polymer during the spray freeze-drying processes used to obtain the Ag-HEC powder sample could have raised its biological reactivity. This hypothesis will need to be further investigated. The Ag-NP positive surface charge has been already demonstrated to be a key factor in determining developmental hazard in Ag-BPEI treated *X. laevis* embryos,[12] likely due to the establishment of the electrostatic interactions with the negatively charged surface of the outer cell membranes.[49] Considering fish embryos, special attention should also be paid to the chorion, an acellular three-layered envelope that surrounds the embryo protecting it from external influences until hatching. Indeed, it has been shown to have negative surface charges[50] and to effectively adsorb Ag leading to up to a 20-fold increase in total Ag concentrations compared to later chorion-free stages.[51] The positive charge provided by the biopolymer not only improved the Ag-HEC NP adhesion to the chorion, but it may have also contributed to facilitating the uptake of Ag into the perivitelline space through the chorion pores.

To all these considerations, the smaller primary size of the novel Ag-HEC NPs compared to the reference ones needs to be considered as another physical property that influences their toxicity. Bar-Ilan *et al.*, using colloidal Ag in a panoply of sizes (3, 10, 50, and 100 nm), demonstrated size dependent effects in which smaller Ag-NPs were more toxic than larger particles in zebrafish embryos.[19] Similarly, Qiang *et al.* considered 4 and 10 nm size range Ag-NPs, showing that only the smallest ones are able to perturb embryonic development following their uptake.[52] The particle size

dependent toxicity could potentially be a function of its relationship to the NP dissolution rate, the amount of reactive surface area, or bioavailability.[53,54] In smaller particles, the higher surface-to-volume ratio increases the proportion of atoms on the surface of the NPs in contact with the test solution or biological matrices leading eventually to higher oxidative dissolution with Ag^+ ion release and ROS production responsible for higher toxicity.[55–58] Although it is still challenging to distinguish whether the toxicity is induced by Ag-NPs themselves or by Ag^+,[8] in our study no association emerged between the NP size and lethality and sub-lethality endpoints, but a positive association of FET toxicity outcomes with dissolved ions can be hypothesised. This suggested, with due caution, that the latter could be relevant in the toxicity of the tested NPs. This association emerged despite the low concentration of Ag measured in the FET solution by ICP-OES analysis, likely due to the formation of complexes and precipitates by the Ag ions eventually released by the NPs, caused by the high chloride content of this solution. These precipitates as well as the NPs were excluded from the quantitative analysis since we applied a static dissolution protocol. This condition does not differ from what could happen in natural water where Ag^+ ions can have a strong tendency to associate with negatively charged ions (*i.e.* chloride, sulphate and fluoride) or complex with humic substances leading to a decrease of Ag-NP toxicity.[59,60] However, the higher toxicity of Ag-HEC NPs with respect to naked or PVP-Ag NPs cannot be justified only on the basis of the soluble fraction of Ag measured in FET solution. Boyle and Goss, evidencing that the total Ag in zebrafish digests was consistently higher for embryos exposed to Ag-NPs than for those exposed to $AgNO_3$, suggested that the chemistry of microenvironments such as the chorion, perivitelline fluid or epithelia where NPs accumulate is likely important to the delivery and release of soluble Ag at its site of toxicity.[32] In support of the above process, studies have shown that after exposure to metal oxide NPs, the chorion can actively accumulate and sequester metal ions in the perivitelline fluid due to the presence of different proteins within it.[41,61–63] The accumulation of exogenous ions makes the perivitelline space an unfavorable microenvironment for the embryo development. In fact, it was demonstrated that although the chorion acts as a barrier blocking the passage of NPs, exposure to different types of Ag-NPs causes similar or even greater toxicity in embryos with chorions than in dechorionated ones.[64,65] These findings are intriguing for understanding the role of the chorion in increasing or decreasing the toxicity of NMs and raise doubts on the opportunity to always remove the chorion in order not to underestimate their toxicity as suggested by ISO 22082:2020.[66] The interaction with biological matrices such as the chorion during the early stages of development could therefore be crucial for Ag-NP oxidative dissolution reactions and HEC could facilitate this interaction.

In our study, granular agglomerates covering the outer surface of the chorion were observed in 48 hpf embryos and, although the hydrodynamic size of all NPs was smaller than the pore size of the chorion of 0.5–0.7 μm, only random passage through chorionic pores of naked and Ag-HEC NPs was evidenced. In addition, no Ag accumulation was detectable in 96 hpf larvae after hatching, indicating low bioavailability of Ag-NPs. Consistent with our findings, Böhme *et al.* demonstrated that Ag-NPs strongly associate with the chorion and substantial amounts seem to reach the perivitelline space, whereas only minor amounts reach the embryo.[67] Similarly, Auffan *et al.* reported that after 48 h of exposure to 5 mg L^{-1} Ag-NPs, the zebrafish chorion adsorbed 58–85% Ag-NPs.[68]

The exposure to all tested Ag-NPs caused morphological alterations of the outer and inner surfaces of the chorion with the formation of deposits apparently attributable to the mucous material and the enlargement of the pore structure as observed by SEM analysis. Chen *et al.* suggested that these modifications could be related to NP and chorionic glycoprotein interaction reducing the barrier effect of the chorion against microorganisms, toxins, and other environmental stresses.[69] Nevertheless, it cannot be excluded that damage to the chorion and blocking of chorion pore canals by larger sized agglomerates have the potential to also reduce gas exchange creating hypoxic conditions in the inner chorionic space that affected embryo development. One of the consequences of this hypoxia has been associated with premature hatching of the embryos,[70,71] a response that we observed at the highest concentrations of Ag-HEC NPs.

Interestingly, Ag-HECp caused delayed hatching, in agreement with the results obtained at high concentrations (50–100 mg L^{-1}) of Ag-BSA and Ag-starch NPs[18] and at 10 mg L^{-1} maltose & gelatine Ag-NPs.[72] Pearson's correlation analysis associated delayed hatching with positive ζ-potential and malformed phenotypes, suggesting that different surface charges have indeed a relevant role in determining interactions and effects in our testing model. A substantial limited effect on the hatching process observed for the two reference Ag-NPs is instead in agreement with Yoo *et al.*[73]

The occurrence of systemic teratogenicity was similar in all Ag-NPs tested with severe dysmorphologies such as bent and twisted notochord, pericardial edema, craniofacial and eye abnormalities, deformation and edema of the yolk sac as reported in previous papers testing different Ag-NPs.[18,74–76] The similar spectrum of malformations among the various types of Ag-NPs is indicative of a similar mode of action of the Ag, which is expressed at different concentrations in relation to the different p-chem characteristics of the NPs. The most noticeable morphological outcome that we observed was a concentration dependent non-depleted yolk sac associated with stunted growth of the embryos. This phenotype mentioned only by some authors[19,52,73] among the sub-lethal signs has so far been underestimated. Since zebrafish embryos are closed systems until 120 hpf relying on endotrophic yolk reserve mobilization for their development, we chose to investigate the retention of neutral lipids in the yolk sac and their distribution in the vasculature, heart, head

and swim bladder by ORO staining as a marker of yolk consumption.[77] The pale ORO staining of blood vessels observed in all treated embryos, particularly in Ag-HEC NPs, indicates a reduction in circulating plasma lipids compared to the control embryos. Since the yolk syncytial layer (YSL) is known to be involved in the degradation and transfer of yolk sac reserves to the embryo and growing larva *via* the circulatory system,[78] this could be the result of an alteration of the activity of this extraembryonic structure induced by exposure to Ag-NPs. Our data indeed resembled in part a clofibrate-induced malabsorption syndrome in zebrafish embryos, resulting from inhibition of the YSL constitutive cell secretion.[79] However, the strong ORO staining evidenced in the cardiac area in the treated *versus* control embryos suggests that pericardial edema may also contribute to decreased lipid transfer into the circulation by reducing blood flow. As described by Fraher *et al.*,[80] who performed a lipidomic analysis of zebrafish embryos, the intensity of ORO staining should gradually decrease in the yolk as development progresses and simultaneously increase in the body of the embryo up to 72 hpf and then be present in traces at 120 hpf. We have not observed this trend in the treated embryos which at 120 hpf still show a well stained yolk and a non-inflated swim bladder indicating a developmental delay.

The inability of the treated embryos to consume their yolk is consistent with the growth retardation evidenced also by the morphometric data that showed a concentration dependent decrease in size of larvae at 96 hpf and analysis of craniofacial cartilages which appear to be developmentally delayed. This hypothesis was supported also by the strong negative Pearson coefficient between the embryo growth parameters and the yolk area. Whether the reduced yolk depletion is due to a defective YSL nutrient transport or to cardiac defects, causing circulatory impairment, needs to be deeply investigated and will be the subject of subsequent studies.

5. Conclusion

In conclusion, toxicity results coupled with correlation analysis of adverse effects with Ag-NP p-chem properties allow us to assume that the surface chemistry and the positive ζ potential are the relevant key factors affecting the zebrafish embryo health. HEC, despite being a green and safe polymer, seems to confer bio-interactive related properties to Ag-NPs that, together with their small size and positive ζ potential, increase their biological reactivity towards zebrafish embryos, reducing the concentrations at which lethal and sublethal outcomes appear.

However, the LC_{50} and EC_{50} values of Ag-HEC NPs measured in mg L^{-1} stand well above natural surface water concentrations quantified in ng L^{-1} and their application as antimicrobials in end-use products should take into account the balance between risks and benefits, considering the effective concentration in non-target organisms *versus* the minimal inhibitory or bactericidal concentration. Obviously, due to the rapid increase in the use and production of Ag-NPs, environmental levels of Ag-NPs are expected to experience an exponential increase, which needs to be factored into decision-making processes.

Considering the sublethal endpoints induced by Ag-NPs, the decrease of yolk lipid consumption is reported here for the first time and deserves to be further investigated.

In the framework of the ASINA project, the introduction of Ag-HEC design options did not satisfy the expected improvement of the safety profile but revealed an interesting correlation of surface chemistry and the colloidal properties with the identified embryo adverse effects, suggesting design criteria for exploiting advantageously the toxicity against undesired biological targets.

Author contributions

P. B. and A. C.: conceptualization, methodology, formal analysis, writing original draft, manuscript review & editing; R. B.: p-chem analysis, manuscript review and editing; M. G.: writing, manuscript review and editing, formal analysis; I. Z.: ICP-OES analysis and revision of the chemical data; M. B. and A. C.: Ag-HEC NP synthesis and ICP-OES data interpretation, manuscript review; P. M.: writing, manuscript review and editing, project administration, and funding acquisition.

Conflicts of interest

There are no conflicts to declare.

Acknowledgements

This work was supported by funding from the European Union for the projects "ASINA" (Anticipating Safety Issues at the Design Stage of Nano Product Development) (H2020—862444) and INTEGRANO (Multidimensional Integrated Quantitative Approach to Assess Safety and Sustainability of Nanomaterials in Real Case Life Cycle Scenarios Using Nanospecific Impact Categories) (Horizon Europe—101138414). The authors wish to thank Dr. Melissa Saibene and Dr. Tiziano Catelani ("Piattaforma Interdipartimentale di Microscopia" of the University of Milan –Bicocca) for the TEM and SEM images and Paola Ghislanzoni and Dr Christian D'Abramo for technical assistance.

References

1 P. Garg, P. Attri, R. Sharma, M. Chauhan and G. R. Chaudhary, Advances and Perspective on Antimicrobial Nanomaterials for Biomedical Applications, *Front. nanotechnol.*, 2022, **4**, DOI: **10.3389/fnano.2022.898411**.

2 S. M. Imani, L. Ladouceur, T. Marshall, R. Maclachlan, L. Soleymani and T. F. Didar, Antimicrobial Nanomaterials and Coatings: Current Mechanisms and Future Perspectives to

Control the Spread of Viruses Including SARS-CoV-2, *ACS Nano*, 2020, **14**, 12341–12369.
3 K. Gold, B. Slay, M. Knackstedt and A. K. Gaharwar, Antimicrobial Activity of Metal and Metal-Oxide Based Nanoparticles, *Adv. Ther.*, 2018, **1**, DOI: **10.1002/adtp.201700033**.
4 Y. L. Su, D. Wu, H. P. Xia, C. Y. Zhang, J. H. Shi, K. J. Wilkinson and B. Xie, Metallic nanoparticles induced antibiotic resistance genes attenuation of leachate culturable microbiota: The combined roles of growth inhibition, ion dissolution and oxidative stress, *Environ. Int.*, 2019, **128**, 407–416.
5 I. Tavernaro, S. Dekkers, L. G. Soeteman-Hernandez, P. Herbeck-Engel, C. Noorlander and A. Kraegeloh, Safe-by-Design part II: A strategy for balancing safety and functionality in the different stages of the innovation process, *Nanoimpact*, 2021, **24**, DOI: **10.1016/j.impact.2021.100354**.
6 L. Yan, F. Zhao, J. Wang, Y. Zu, Z. J. Gu and Y. L. Zhao, A Safe-by-Design Strategy towards Safer Nanomaterials in Nanomedicines, *Adv. Mater.*, 2019, **31**, DOI: **10.1002/adma.201805391**.
7 C. Z. Liao, Y. C. Li and S. C. Tjong, Bactericidal and Cytotoxic Properties of Silver Nanoparticles, *Int. J. Mol. Sci.*, 2019, **20**, DOI: **10.3390/ijms20020449**.
8 M. Akter, M. T. Sikder, M. M. Rahman, A. Ullah, K. F. B. Hossain, S. Banik, T. Hosokawa, T. Saito and M. Kurasaki, A systematic review on silver nanoparticles-induced cytotoxicity: Physicochemical properties and perspectives, *J. Adv. Res.*, 2018, **9**, 1–16.
9 Z. Ferdous and A. Nemmar, Health Impact of Silver Nanoparticles: A Review of the Biodistribution and Toxicity Following Various Routes of Exposure, *Int. J. Mol. Sci.*, 2020, **21**, DOI: **10.3390/ijms21072375**.
10 B. Le Ouay and F. Stellacci, Antibacterial activity of silver nanoparticles: A surface science insight, *Nano Today*, 2015, **10**, 339–354.
11 K. W. H. Kwok, W. Dong, S. M. Marinakos, J. Liu, A. Chilkoti, M. R. Wiesner, M. Chernick and D. E. Hinton, Silver nanoparticle toxicity is related to coating materials and disruption of sodium concentration regulation, *Nanotoxicology*, 2016, **10**, 1306–1317.
12 A. Colombo, M. Saibene, E. Moschini, P. Bonfanti, M. Collini, K. Kasemets and P. Mantecca, Teratogenic hazard of BPEI-coated silver nanoparticles to *Xenopus laevis*, *Nanotoxicology*, 2017, **11**, 405–418.
13 S. Makama, S. K. Kloet, J. Piella, H. van den Berg, N. C. A. de Ruijter, V. F. Puntes, I. Rietjens and N. W. van den Brink, Effects of Systematic Variation in Size and Surface Coating of Silver Nanoparticles on Their In Vitro Toxicity to Macrophage RAW 264.7 Cells, *Toxicol. Sci.*, 2018, **162**, 79–88.
14 L. B. Ahmed, M. Millic, I. M. Pongrac, A. M. Marjanovic, H. Mlinaric, I. Pavicic, S. Gajovic and I. V. Vrcek, Impact of surface functionalization on the uptake mechanism and toxicity effects of silver nanoparticles in HepG2 cells, *Food Chem. Toxicol.*, 2017, **107**, 349–361.
15 S. Ruchika, A. Sharma and A. Saneja, Zebrafish as a powerful alternative model organism for preclinical investigation of nanomedicines, *Drug Discovery Today*, 2022, **27**, 1513–1522.
16 P. D. Noyes, G. R. Garcia and R. L. Tanguay, Zebrafish as an in vivo model for sustainable chemical design, *Green Chem.*, 2016, **18**, 6410–6430.
17 C. Chakraborty, A. R. Sharma, G. Sharma and S. S. Lee, Zebrafish: A complete animal model to enumerate the nanoparticle toxicity, *J. Nanobiotechnol.*, 2016, **14**, DOI: **10.1186/s12951-016-0217-6**.
18 P. V. Asharani, Y. Lian Wu, Z. Gong and S. Valiyaveettil, Toxicity of silver nanoparticles in zebrafish models, *Nanotechnology*, 2008, **19**, 255102.
19 O. Bar-Ilan, R. M. Albrecht, V. E. Fako and D. Y. Furgeson, Toxicity assessments of multisized gold and silver nanoparticles in zebrafish embryos, *Small*, 2009, **5**, 1897–1910.
20 C. M. Powers, E. D. Levin, F. J. Seidler and T. A. Slotkin, Silver exposure in developing zebrafish produces persistent synaptic and behavioral changes, *Neurotoxicol. Teratol.*, 2011, **33**, 329–332.
21 A. Massarsky, L. Dupuis, J. Taylor, S. Eisa-Beygi, L. Strek, V. L. Trudeau and T. W. Moon, Assessment of nanosilver toxicity during zebrafish (*Danio rerio*) development, *Chemosphere*, 2013, **92**, 59–66.
22 L. M. Browning, K. J. Lee, P. D. Nallathamby and X. H. Xu, Silver nanoparticles incite size- and dose-dependent developmental phenotypes and nanotoxicity in zebrafish embryos, *Chem. Res. Toxicol.*, 2013, **26**, 1503–1513.
23 R. van Aerle, A. Lange, A. Moorhouse, K. Paszkiewicz, K. Ball, B. D. Johnston, E. de-Bastos, T. Booth, C. R. Tyler and E. M. Santos, Molecular mechanisms of toxicity of silver nanoparticles in zebrafish embryos, *Environ. Sci. Technol.*, 2013, **47**, 8005–8014.
24 A. L. Costa, M. Blosi, A. Brigliadori, I. Zanoni, S. Ortelli, F. C. Simeone, S. Delbue, S. D'Alessandro, S. Parapini, C. Vineis, A. Varesano, M. S. Toprak, B. Hamawandi and D. Gardini, Eco design for Ag-based solutions against SARS-CoV-2 and E. coli, *Environ. Sci.: Nano*, 2022, **9**, 4295–4304.
25 S. Trabucco, S. Ortelli, B. Del Secco, I. Zanoni, F. Belosi, F. Ravegnani, A. Nicosia, M. Blosi and A. L. Costa, Monitoring and Optimisation of Ag Nanoparticle Spray-Coating on Textiles, *Nanomaterials*, 2021, **11**, DOI: **10.3390/nano11123165**.
26 V. Marassi, L. Di Cristo, S. G. J. Smith, S. Ortelli, M. Blosi, A. L. Costa, P. Reschiglian, Y. Volkov and A. Prina-Mello, Silver nanoparticles as a medical device in healthcare settings: a five-step approach for candidate screening of coating agents, *R. Soc. Open Sci.*, 2018, **5**, DOI: **10.1098/rsos.171113**.
27 OECD, *Test No. 236: Fish embryo acute toxicity (FET) test. Guidelines for the Testing of Chemicals*, Paris, France, 2013, DOI: **10.1787/9789264203709-en**.
28 D. Gardini, M. Blosi, S. Ortelli, C. Delpivo, O. Bussolati, M. G. Bianchi, M. Allegri, E. Bergamaschi and A. L. Costa, Nanosilver: An innovative paradigm to promote its safe and active use, *Nanoimpact*, 2018, **11**, 128–135.

29 M. Blosi, S. Albonetti, M. Dondi, G. Baldi, A. Barzanti and M. Bitossi, Process for Preparing Stable Suspensions of Metal Nanoparticles and the Stable Colloidal Suspensions Obtained Thereby, *European Patent Office*, EP2403636A2, 2010.

30 G. Motta, M. Gualtieri, M. Saibene, R. Bengalli, A. Brigliadori, M. Carriere and P. Mantecca, Preliminary Toxicological Analysis in a Safe-by-Design and Adverse Outcome Pathway-Driven Approach on Different Silver Nanoparticles: Assessment of Acute Responses in A549 Cells, *Toxics*, 2023, **11**, DOI: **10.3390/toxics11020195**.

31 E. Commission, Directive 2010/63/EU of the European Parliament and of the Council of 22 September 2010 on the protection of animals used for scientific purposes, *Official Journal of the European Union*, 2010, L276.

32 D. Boyle and G. G. Goss, Effects of silver nanoparticles in early life-stage zebrafish are associated with particle dissolution and the toxicity of soluble silver, *Nanoimpact*, 2018, **12**, 1–8.

33 J. Karlsson, J. von Hofsten and P. E. Olsson, Generating transparent zebrafish: A refined method to improve detection of gene expression during embryonic development, *Mar. Biotechnol.*, 2001, **3**, 522–527.

34 C. Cornet, S. Calzolari, R. Minana-Prieto, S. Dyballa, E. van Doornmalen, H. Rutjes, T. Savy, D. D'Amico and J. Terriente, ZeGlobalTox: An Innovative Approach to Address Organ Drug Toxicity Using Zebrafish, *Int. J. Mol. Sci.*, 2017, **18**, 864.

35 P. Bonfanti, M. Saibene, R. Bacchetta, P. Mantecca and A. Colombo, A glyphosate micro-emulsion formulation displays teratogenicity in *Xenopus laevis*, *Aquat. Toxicol.*, 2018, **195**, 103–113.

36 D. J. Finney, *Probit Analysis*, 3rd edn, 1971.

37 F. E. Harrell Jr and C. Dupont, Harrell Miscellaneous, *R package version 5.1-1*, 2023.

38 S. Jarque, M. Rubio-Brotons, J. Ibarra, V. Ordonez, S. Dyballa, R. Minana and J. Terriente, Morphometric analysis of developing zebrafish embryos allows predicting teratogenicity modes of action in higher vertebrates, *Reprod. Toxicol.*, 2020, **96**, 337–348.

39 H. T. Ratte, Bioaccumulation and toxicity of silver compounds: A review, *Environ. Toxicol. Chem.*, 1999, **18**, 89–108.

40 R. J. Griffitt, J. Luo, J. Gao, J. C. Bonzongo and D. S. Barber, Effects of particle composition and species on toxicity of metallic nanomaterials in aquatic organisms, *Environ. Toxicol. Chem.*, 2008, **27**, 1972–1978.

41 S. J. Lin, Y. Zhao, T. Xia, H. Meng, Z. X. Ji, R. Liu, S. George, S. J. Xiong, X. Wang, H. Y. Zhang, S. Pokhrel, L. Madler, R. Damoiseaux, S. Lin and A. E. Nel, High Content Screening in Zebrafish Speeds up Hazard Ranking of Transition Metal Oxide Nanoparticles, *ACS Nano*, 2011, **5**, 7284–7295.

42 G. R. Tortella, O. Rubilar, N. Durán, M. C. Diez, M. Martínez, J. Parada and A. B. Seabra, Silver nanoparticles: Toxicity in model organisms as an overview of its hazard for human health and the environment, *J. Hazard. Mater.*, 2020, **390**, DOI: **10.1016/j.jhazmat.2019.121974**.

43 J. M. Clark, The 3Rs in research: a contemporary approach to replacement, reduction and refinement, *Br. J. Nutr.*, 2018, **120**, S1–S7.

44 U. Strahle, S. Scholz, R. Geisler, P. Greiner, H. Hollert, S. Rastegar, A. Schumacher, I. Selderslaghs, C. Weiss, H. Witters and T. Braunbeck, Zebrafish embryos as an alternative to animal experiments-A commentary on the definition of the onset of protected life stages in animal welfare regulations, *Reprod. Toxicol.*, 2012, **33**, 128–132.

45 F. Gottschalk, C. Lassen, J. Kjoelholt, F. Christensen and B. Nowack, Modeling Flows and Concentrations of Nine Engineered Nanomaterials in the Danish Environment, *Int. J. Environ. Res. Public Health*, 2015, **12**, 5581–5602.

46 R. Ramirez, V. Marti and R. M. Darbra, Environmental Risk Assessment of Silver Nanoparticles in Aquatic Ecosystems Using Fuzzy Logic, *Water*, 2022, **14**, DOI: **10.3390/w14121885**.

47 J. G. Cho, K. T. Kim, T. K. Ryu, J. W. Lee, J. E. Kim, J. Kim, B. C. Lee, E. H. Jo, J. Yoon, I. C. Eom, K. Choi and P. Kim, Stepwise Embryonic Toxicity of Silver Nanoparticles on *Oryzias latipes*, *BioMed Res. Int.*, 2013, **2013**, DOI: **10.1155/2013/494671**.

48 J. Ciekot, M. Psurski, K. Jurec and J. Boratynski, Hydroxyethylcellulose as a methotrexate carrier in anticancer therapy, *Invest. New Drugs*, 2021, **39**, 15–23.

49 K. Jain, P. Kesharwani, U. Gupta and N. K. Jain, Dendrimer toxicity: Let's meet the challenge, *Int. J. Pharm.*, 2010, **394**, 122–142.

50 N. H. Hart and M. Donovan, FINE-STRUCTURE OF THE CHORION AND SITE OF SPERM ENTRY IN THE EGG OF BRACHYDANIO, *J. Exp. Zool.*, 1983, **227**, 277–296.

51 S. Bohme, H. J. Stark, T. Reemtsma and D. Kuhnel, Effect propagation after silver nanoparticle exposure in zebrafish (Danio rerio) embryos: a correlation to internal concentration and distribution patterns, *Environ. Sci.: Nano*, 2015, **2**, 603–614.

52 L. Y. Qiang, Z. H. Arabeyyat, Q. Xin, V. N. Paunov, I. J. F. Dale, R. I. L. Mills, J. M. Rotchell and J. P. Cheng, Silver Nanoparticles in Zebrafish (*Danio rerio*) Embryos: Uptake, Growth and Molecular Responses, *Int. J. Mol. Sci.*, 2020, **21**, DOI: **10.3390/ijms21051876**.

53 S. K. Misra, A. Dybowska, D. Berhanu, S. N. Luoma and E. Valsami-Jones, The complexity of nanoparticle dissolution and its importance in nanotoxicological studies, *Sci. Total Environ.*, 2012, **438**, 225–232.

54 A. Orbea, N. Gonzalez-Soto, J. M. Lacave, I. Barrio and M. P. Cajaraville, Developmental and reproductive toxicity of PVP/PEI-coated silver nanoparticles to zebrafish, *Comp. Biochem. Physiol., Part C: Toxicol. Pharmacol.*, 2017, **199**, 59–68.

55 W. Zhang, Y. Yao, N. Sullivan and Y. S. Chen, Modeling the Primary Size Effects of Citrate-Coated Silver Nanoparticles on Their Ion Release Kinetics, *Environ. Sci. Technol.*, 2011, **45**, 4422–4428.

56 R. Ma, C. Levard, S. M. Marinakos, Y. W. Cheng, J. Liu, F. M. Michel, G. E. Brown and G. V. Lowry, Size-Controlled Dissolution of Organic-Coated Silver Nanoparticles, *Environ. Sci. Technol.*, 2012, **46**, 752–759.

57 C. Carlson, S. M. Hussain, A. M. Schrand, L. K. Braydich-Stolle, K. L. Hess, R. L. Jones and J. J. Schlager, Unique Cellular Interaction of Silver Nanoparticles: Size-Dependent Generation of Reactive Oxygen Species, *J. Phys. Chem. B*, 2008, **112**, 13608–13619.

58 S. Bakand and A. Hayes, Toxicological Considerations, Toxicity Assessment, and Risk Management of Inhaled Nanoparticles, *Int. J. Mol. Sci.*, 2016, **17**, DOI: **10.3390/ijms17060929**.

59 K. J. Groh, T. Dalkvist, F. Piccapietra, R. Behra, M. J. F. Suter and K. Schirmer, Critical influence of chloride ions on silver ion-mediated acute toxicity of silver nanoparticles to zebrafish embryos, *Nanotoxicology*, 2015, **9**, 81–91.

60 P. R. Caceres-Velez, M. L. Fascineli, M. H. Sousa, C. K. Grisolia, L. Yate, P. E. N. de Souza, I. Estrela-Lopis, S. Moya and R. B. Azevedo, Humic acid attenuation of silver nanoparticle toxicity by ion complexation and the formation of a Ag^{3+} coating, *J. Hazard. Mater.*, 2018, **353**, 173–181.

61 T. A. Xia, Y. Zhao, T. Sager, S. George, S. Pokhrel, N. Li, D. Schoenfeld, H. A. Meng, S. J. Lin, X. Wang, M. Y. Wang, Z. X. Ji, J. I. Zink, L. Madler, V. Castranova, S. Lin and A. E. Nel, Decreased Dissolution of ZnO by Iron Doping Yields Nanoparticles with Reduced Toxicity in the Rodent Lung and Zebrafish Embryos, *ACS Nano*, 2011, **5**, 1223–1235.

62 J. Hua, M. G. Vijver, F. Ahmad, M. K. Richardson and W. Peijnenburg, Toxicity Of Different-Sized Copper Nano-And Submicron Particles And Their Shed Copper Ions To Zebrafish Embryos, *Environ. Toxicol. Chem.*, 2014, **33**, 1774–1782.

63 E. B. Muller, S. J. Lin and R. M. Nisbet, Quantitative Adverse Outcome Pathway Analysis of Hatching in Zebrafish with CuO Nanoparticles, *Environ. Sci. Technol.*, 2015, **49**, 11817–11824.

64 S. Cunningham, M. E. Brennan-Fournet, D. Ledwith, L. Byrnes and L. Joshi, Effect of Nanoparticle Stabilization and Physicochemical Properties on Exposure Outcome: Acute Toxicity of Silver Nanoparticle Preparations in Zebrafish (Danio rerio), *Environ. Sci. Technol.*, 2013, **47**, 3883–3892.

65 K. Park, G. Tuttle, F. Sinche and S. L. Harper, Stability of citrate-capped silver nanoparticles in exposure media and their effects on the development of embryonic zebrafish (Danio rerio), *Arch. Pharmacal Res.*, 2013, **36**, 125–133.

66 International Organization for Standardization (ISO), Assessment of nanaomaterial toxicity using dechorionated zebrafish embryo, *Nanotechnologies ISO/TS 22082*, 2020.

67 S. Böhme, M. Baccaro, M. Schmidt, A. Potthoff, H. J. Stärk, T. Reemtsma and D. Kühnel, Metal uptake and distribution in the zebrafish (Danio rerio) embryo: differences between nanoparticles and metal ions, *Environ. Sci.: Nano*, 2017, **4**, 1005–1015.

68 M. Auffan, C. W. Matson, J. Rose, M. Arnold, O. Proux, B. Fayard, W. Liu, P. Chaurand, M. R. Wiesner, J. Y. Bottero and R. T. Di Giulio, Salinity-dependent silver nanoparticle uptake and transformation by Atlantic killifish (Fundulus heteroclitus) embryos, *Nanotoxicology*, 2014, **8**, 167–176.

69 Z. Y. Chen, N. J. Li, F. Y. Cheng, J. F. Hsueh, C. C. Huang, F. I. Lu, T. F. Fu, S. J. Yan, Y. H. Lee and Y. J. Wang, The Effect of the Chorion on Size-Dependent Acute Toxicity and Underlying Mechanisms of Amine-Modified Silver Nanoparticles in Zebrafish Embryos, *Int. J. Mol. Sci.*, 2020, **21**, DOI: **10.3390/ijms21082864**.

70 G. Malafaia, A. M. de Souza, A. C. Pereira, S. Gonçalves, A. P. D. Araújo, R. X. Ribeiro and T. L. Rocha, Developmental toxicity in zebrafish exposed to polyethylene microplastics under static and semi-static aquatic systems, *Sci. Total Environ.*, 2020, **700**, DOI: **10.1016/j.scitotenv.2019.134867**.

71 A. C. Pereira, B. B. Gonçalves, R. D. Brito, L. G. Vieira, E. C. D. Lima and T. L. Rocha, Comparative developmental toxicity of iron oxide nanoparticles and ferric chloride to zebrafish (Danio rerio) after static and semi-static exposure, *Chemosphere*, 2020, **254**, DOI: **10.1016/j.chemosphere.2020.126792**.

72 H. Caloudova, N. Hodkovicova, P. Sehonova, J. Blahova, B. Marsalek, A. Panacek and Z. Svobodova, The effect of silver nanoparticles and silver ions on zebrafish embryos *Danio rerio*, *Neuroendocrinol. Lett.*, 2018, **39**, 299–304.

73 M. H. Yoo, Y. C. Rah, J. Choi, S. Park, H. C. Park, K. H. Oh, S. H. Lee and S. Y. Kwon, Embryotoxicity and and hair cell toxicity of silver nanoparticles in zebrafish embryos, *Int. J. Pediatr. Otorhinolaryngol.*, 2016, **83**, 168–174.

74 G. Q. Xia, T. T. Liu, Z. W. Wang, Y. Hou, L. H. Dong, J. Y. Zhu and J. Qi, The effect of silver nanoparticles on zebrafish embryonic development and toxicology, *Artif. Cells, Nanomed., Biotechnol.*, 2016, **44**, 1116–1121.

75 S. George, T. A. Xia, R. Rallo, Y. Zhao, Z. X. Ji, S. J. Lin, X. Wang, H. Y. Zhang, B. France, D. Schoenfeld, R. Damoiseaux, R. Liu, S. Lin, K. A. Bradley, Y. Cohen and A. E. Nel, Use of a High-Throughput Screening Approach Coupled with In Vivo Zebrafish Embryo Screening To Develop Hazard Ranking for Engineered Nanomaterials, *ACS Nano*, 2011, **5**, 1805–1817.

76 D. A. Mosselhy, W. He, D. Li, Y. P. Meng and Q. L. Feng, Silver nanoparticles: in vivo toxicity in zebrafish embryos and a comparison to silver nitrate, *J. Nanopart. Res.*, 2016, **18**, 222.

77 A. Schlegel and D. Y. R. Stainier, Microsomal triglyceride transfer protein is required for yolk lipid utilization and absorption of dietary lipids in zebrafish larvae, *Biochemistry*, 2006, **45**, 15179–15187.

78 G. Poupard, M. André, M. Durliat, C. Ballagny, G. Boeuf and P. J. Babin, Apolipoprotein E gene expression correlates with endogenous lipid nutrition and yolk syncytial layer lipoprotein synthesis during fish development, *Cell Tissue Res.*, 2000, **300**, 251–261.

79 D. Raldua, M. André and P. J. Babin, Clofibrate and gemfibrozil induce an embryonic malabsorption syndrome in zebrafish, *Toxicol. Appl. Pharmacol.*, 2008, **228**, 301–314.

80 D. Fraher, A. Sanigorski, N. A. Mellett, P. J. Meikle, A. J. Sinclair and Y. Gibert, Zebrafish Embryonic Lipidomic Analysis Reveals that the Yolk Cell Is Metabolically Active in Processing Lipid, *Cell Rep.*, 2016, **14**, 1317–1329.